Nuclear clustering and pasta in neutron stars

Nicolas Chamel
Université Libre de Bruxelles, Belgium

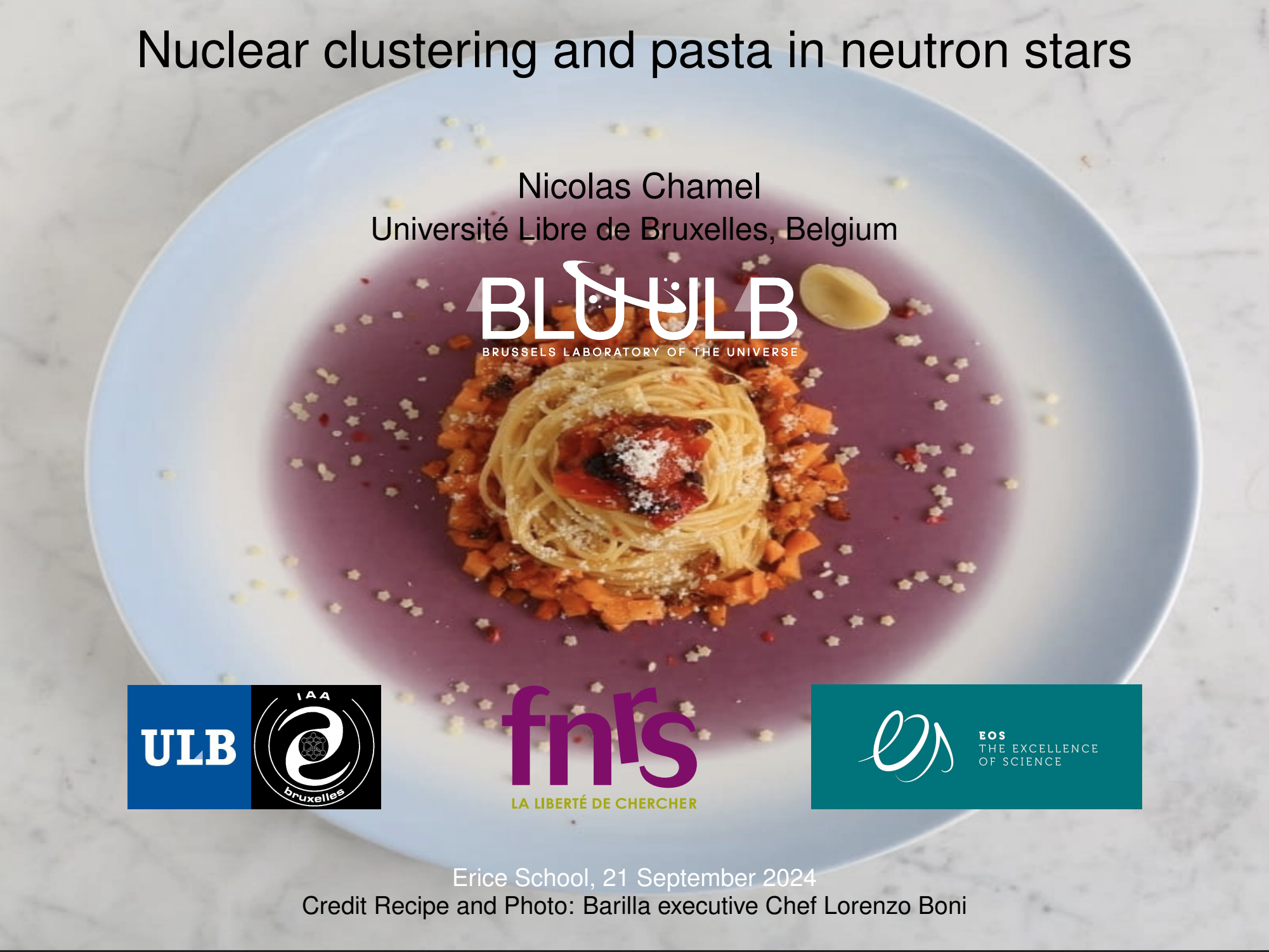

Erice School, 21 September 2024

Credit Recipe and Photo: Barilla executive Chef Lorenzo Boni

Nuclear pasta recipe: angel hair with carrots

Ingredients:

- 1 box Barilla Angel Hair
- 6 tbs. extra-virgin olive oil, divided
- 2 carrots, peeled and diced into small pieces
- 2 red bell peppers, diced into small pieces
- 1/2 cup Romano cheese
- Salt and black pepper, to taste

Italian Chef Lorenzo Boni © 2019 Copyright Live Naturally

Ingredients for the Garnish:

- A few pieces of cooked Barilla Collezione Orecchiette
- 2 tbs. Barilla Pastina, cooked and drained

Directions:

1. Turn on the oven and set to 230 °C.
2. Season the carrots and peppers separately with 2 tbs. of olive oil, salt, pepper.
3. Place the seasoned vegetables on a sheet pan and roast in the oven $\sim$ 20'.
4. Cook pasta according to the package directions and then drain and toss with remaining olive oil and cheese.
5. Garnish with vegetables before serving.

Credit Recipe: Barilla executive Chef Lorenzo Boni


Spoiler alert!
generated by Microsoft Copilot

Neutron stars

Neutron stars are not “stars”: they are the extremely compact remnants of gravitational core-collapse supernova explosions.

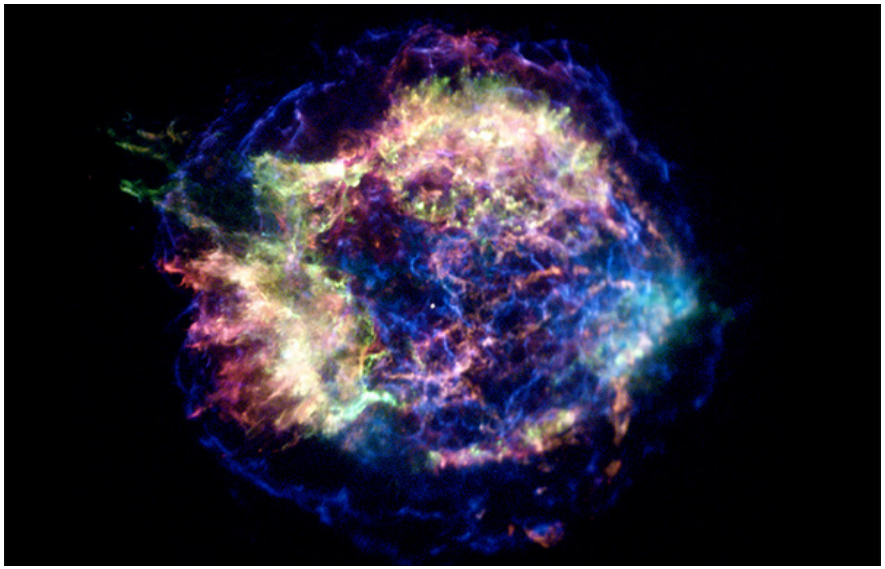

Nuclear physics:

$M \sim 1 - 2M_\odot$
$R \sim 10$ km
$\Rightarrow \rho \sim 10^{15}$ g cm^{-3}

Energy scale: MeV

“cold” $\lesssim 10^{10}$ K $\lesssim$ “hot”

Neutron stars are initially very hot ($\sim 10^{12}$ K) but cool down to $\sim 10^9$ K within days by releasing neutrinos:

cold “catalyzed” matter hypothesis
matter in full thermodynamic equilibrium (ground state)
Harrison, Wakano and Wheeler, Onzième Conseil de Physique Solvay (Stoops, Brussels, Belgium, 1958) pp 124-146

Neutron-star interior

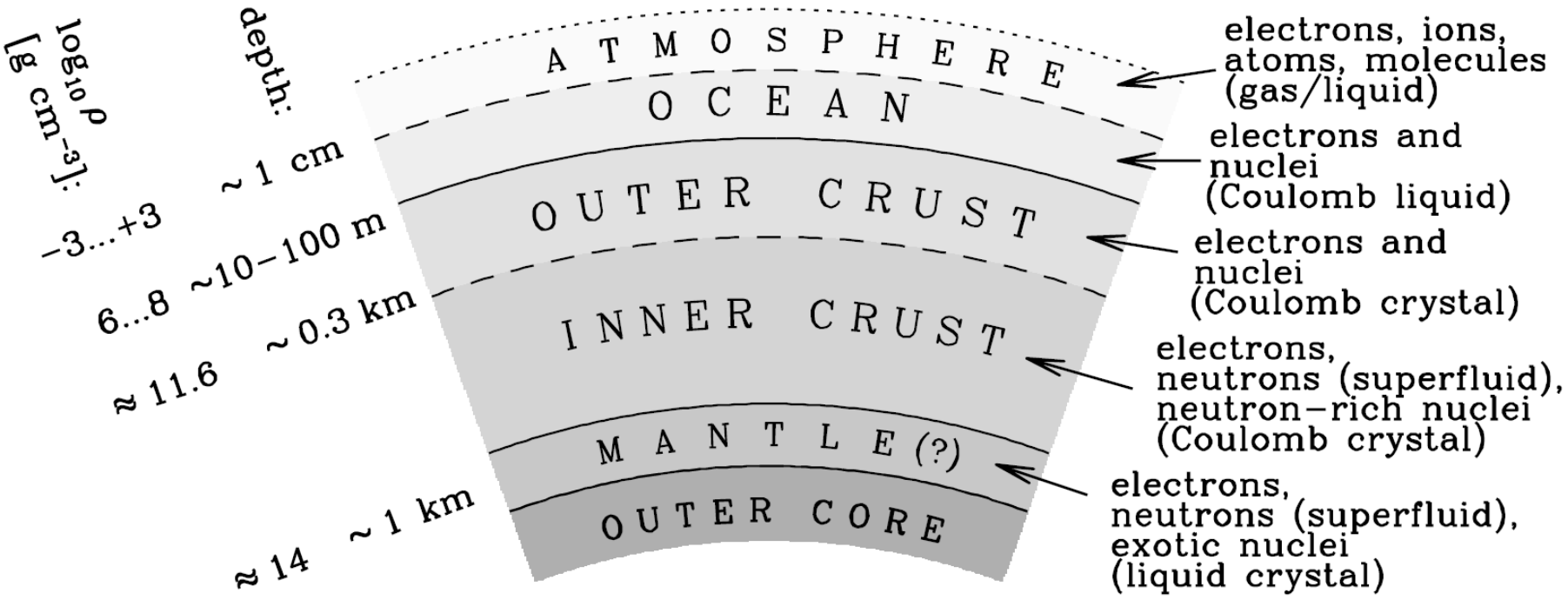

picture taken from Haensel, Potekhin, Yakovlev, "Neutron Stars" (Springer, 2007)

Despite their name, neutron stars are not only made of neutrons!

Blaschke&Chamel, Astrophys. Space Sci. Lib. 457, eds L. Rezzolla, P. Pizzochero, D. I. Jones, N. Rea, I. Vidaña p. 337-400 (Springer, 2018), arXiv:1803.01836

Neutron-star surface

The surface of a neutron star is expected to be made of **iron** (identification of broad Fe K emission lines from accretion disk around neutron stars in low-mass X-ray binaries).

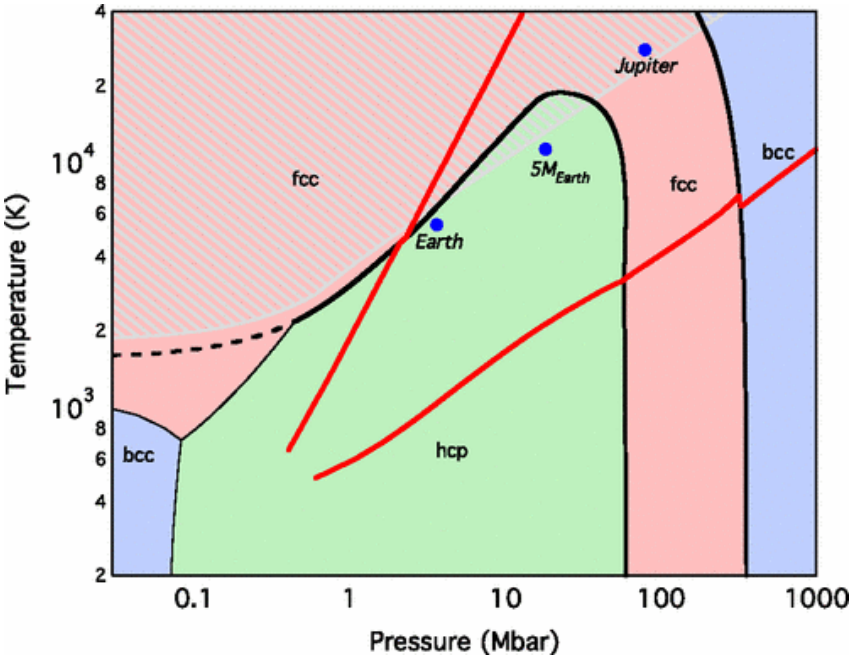

Stixrude, Phys.Rev.Lett. 108, 055505 (2012)

Compressed iron can be studied with **nuclear explosions and laser-driven shock-wave experiments**...

But at pressures corresponding to about **0.1 mm below the surface** (for a star with a mass of $1.4 M_\odot$ and a radius of 12 km)!

Ab initio calculations predict various structural phase transitions: iron is expected to have a **body-centered cubic** (bcc) crystal lattice structure at high pressures.

Crystal Coulomb plasma

At a density $\rho_{\rm eip} \approx 2 \times 10^4$ g cm^{-3} (about 22 cm below the surface), the interatomic spacing becomes comparable with the atomic radius.

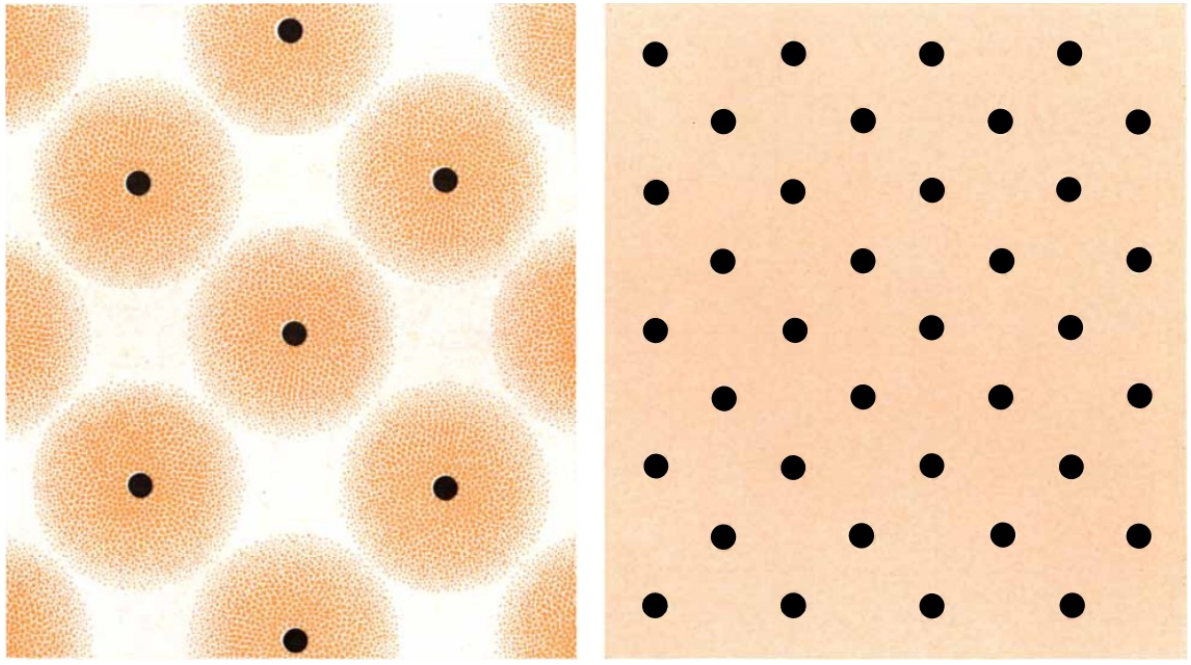

Ruderman, Scientific American 224, 24 (1971)

At densities $\rho \gg \rho_{\rm eip}$, atoms are crushed into a **dense bcc crystal Coulomb plasma of nuclei and free electrons**.

Description of the outer crust of a neutron star

Traditional approach: numerical minimization of the Gibbs free energy per nucleon at different pressures P

Tondeur, A&A 14, 451 (1971); Baym, Pethick, Sutherland, ApJ 170, 299 (1971)

- layers can be easily missed if δP not small enough!
- numerically costly (BPS considered 130 even nuclei vs $\sim 10^4$)

New approach: iterative minimization of the pressures between adjacent crustal layers (approximate analytical formulas)

Chamel, Phys. Rev. C 101, 032801(R) (2020)

computer code: `http://doi.org/10.5281/zenodo.3719439`

- very accurate and reliable ($\delta P/P \sim 10^{-3}$ %)
- composition and stratification (depths, abundances)
- $\sim 10^6$ times faster

Nuclear-physics inputs:
masses of atomic nuclei

Gravitational stratification and matter neutronization

The crust is stratified into **pure layers** composed of nuclei (Z, A). The pressure P is mainly determined by the relativistic electron Fermi gas.

At the interface, $P \approx P_e(n_e)$ therefore n_e must be continuous.

- Electric charge neutrality, $n_e = \dfrac{Z_1}{A_1}\bar{n}_1 = \dfrac{Z_2}{A_2}\bar{n}_2$.
- Hydrostatic equilibrium $\bar{n}_2 > \bar{n}_1 \Rightarrow Z_2/A_2 < Z_1/A_1$.
- $\mu_e^{1\to 2} > 0 \Rightarrow M(A_2, Z_2)/A_2 > M(A_1, Z_1)/A_1$.

Chamel&Fantina,Phys.Rev.C 94, 065802 (2016)

With increasing depth, **nuclei become more neutron rich until neutrons "drip" out** marking the transition to the inner crust, where nuclei coexist with free neutrons and electrons.

Experimentally determined layers

The composition is completely determined by experimental data down to $\sim$ 200m for a $1.4 M_\odot$ neutron star with a radius $R = 10$ km.

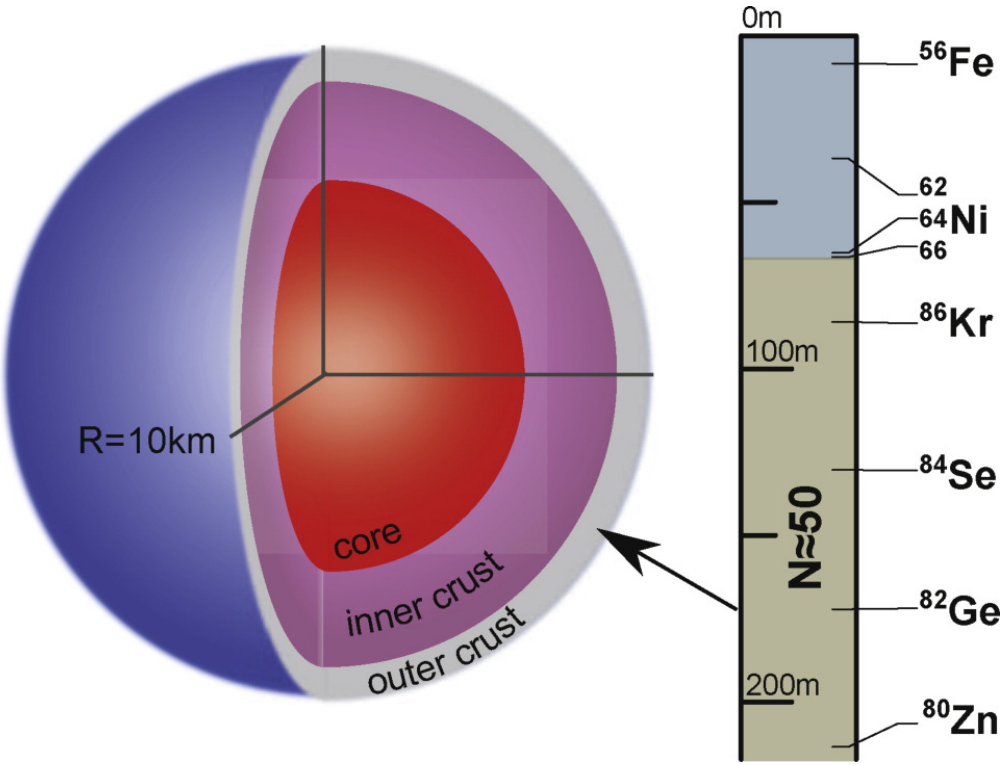

Importance of nuclei with nearly magic N.

Due to β equilibrium and electric charge neutrality, Z is more tightly constrained.

Few layers with $Z = 28$.

Kreim et al., Int.J.M.Spec.349-350,63(2013)

In 1971, the crust was experimentally known down to the layer of ^{84}Se at density 8×10^9 g/cm^{-3}. Nowadays, the limit is at 6×10^{10} g/cm^{-3}.

Plumbing neutron stars to new depths

Precision mass measurements of ^{82}Zn by the ISOLTRAP collaboration at CERN allowed to reach the layer of ^{80}Zn in 2013.

Nuclei in the layers beneath must be such that $Z/A < 0.375$ and $M(A,Z)/A > 930.848$ MeV.

This rules out the doubly magic ^{48}Ca, ^{48}Ni, and ^{56}Ni but not ^{78}Ni.

Errors of a few keV on masses can change the composition.

Pastore et al.,PRC101,035804(2020)

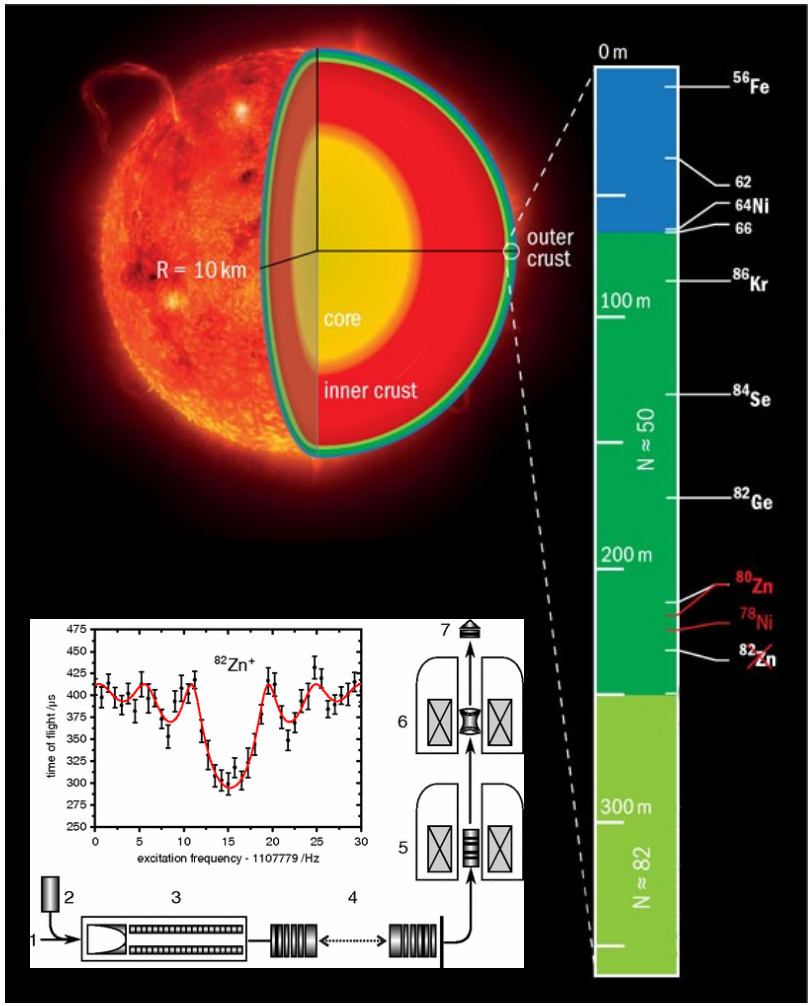

Wolf et al.,Phys.Rev.Lett.110,041101(2013)

Precision mass measurements of nuclei $Z \sim 40$, $N \sim 82$ needed!

Stratigraphic column of the outer crust

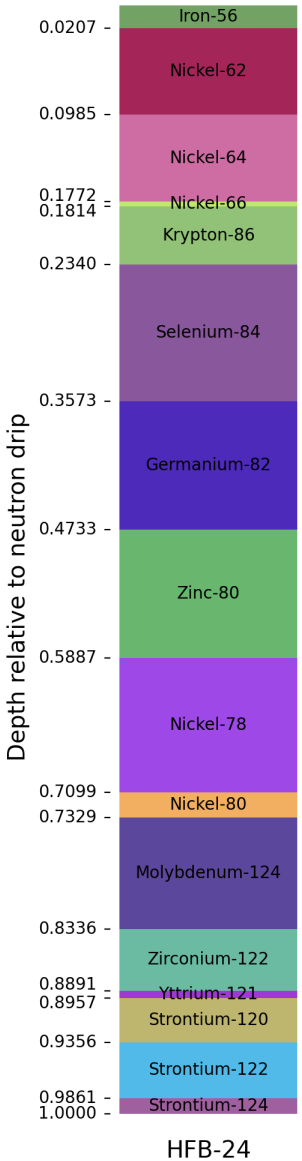

To drill deeper, nuclear mass models must be used:

- semi-empirical (e.g. Bethe & Weizsäcker)
- mic-mac (e.g. Duflo & Zucker, FRDM)
- “microscopic” (e.g. HFB, RMF)

Lunney et al., Rev. Mod. Phys.75, 1021 (2003)

Example shown of the left:

Pearson et al., MNRAS 481, 2994 (2018)

Freely available computer code:

`http://doi.org/10.5281/zenodo.3719439`

Refined mass models using machine learning:

Utama et al., Phys.Rev.C93,014311(2016)

Shelley&Pastore, Universe 7, 131 (2021)

However, such models cannot be used to describe the inner crust and core.

Neutron-drip transition: general considerations

With increasing pressure, nuclei become unstable against **neutron emission induced by electron captures**

$$ {}^{A}_{Z}\mathrm{X} + \Delta Z e^{-} \rightarrow {}^{A-\Delta N}_{Z-\Delta Z}\mathrm{Y} + \Delta N\, n + \Delta Z\, \nu_e $$

Nuclei are stable against neutron emission alone ($\Delta Z = 0, \Delta N \geq 1$)!

	outer crust	drip line	ρ_{drip} (g cm^{-3})	P_{drip} (dyn cm^{-2})
HFB-19	^{126}Sr (0.73)	^{121}Sr (-0.62)	4.40×10^{11}	7.91×10^{29}
HFB-20	^{126}Sr (0.48)	^{121}Sr (-0.71)	4.39×10^{11}	7.89×10^{29}
HFB-21	^{124}Sr (0.83)	^{121}Sr (-0.33)	4.30×10^{11}	7.84×10^{29}

The numbers in parentheses are the neutron separation energies $S_n(A,Z) \equiv M(A-1,Z)c^2 - M(A,Z)c^2 + m_n c^2$ in MeV.

ρ_{drip} and P_{drip} can be expressed by simple analytical formulas.

Chamel et al., Phys. Rev. C91, 055803 (2015)

Nuclei in dense stellar environments

In 1971, Baym, Bethe, and Pethick described nuclei in the inner crust of a neutron star as **nuclear liquid drops in a uniform neutron gas**.

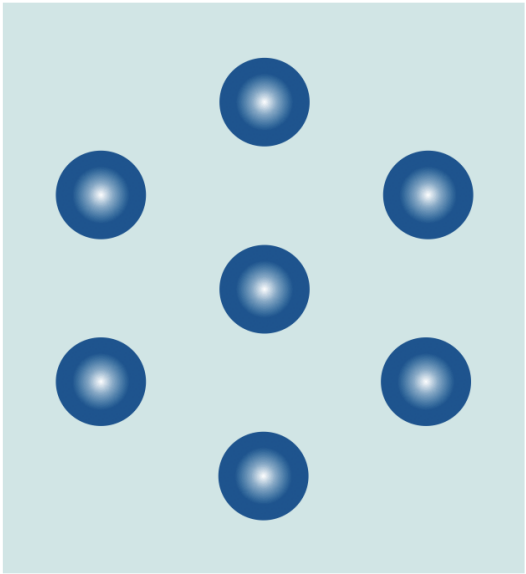

Nuclei in dense stellar environments

In 1971, Baym, Bethe, and Pethick described nuclei in the inner crust of a neutron star as **nuclear liquid drops in a uniform neutron gas**.

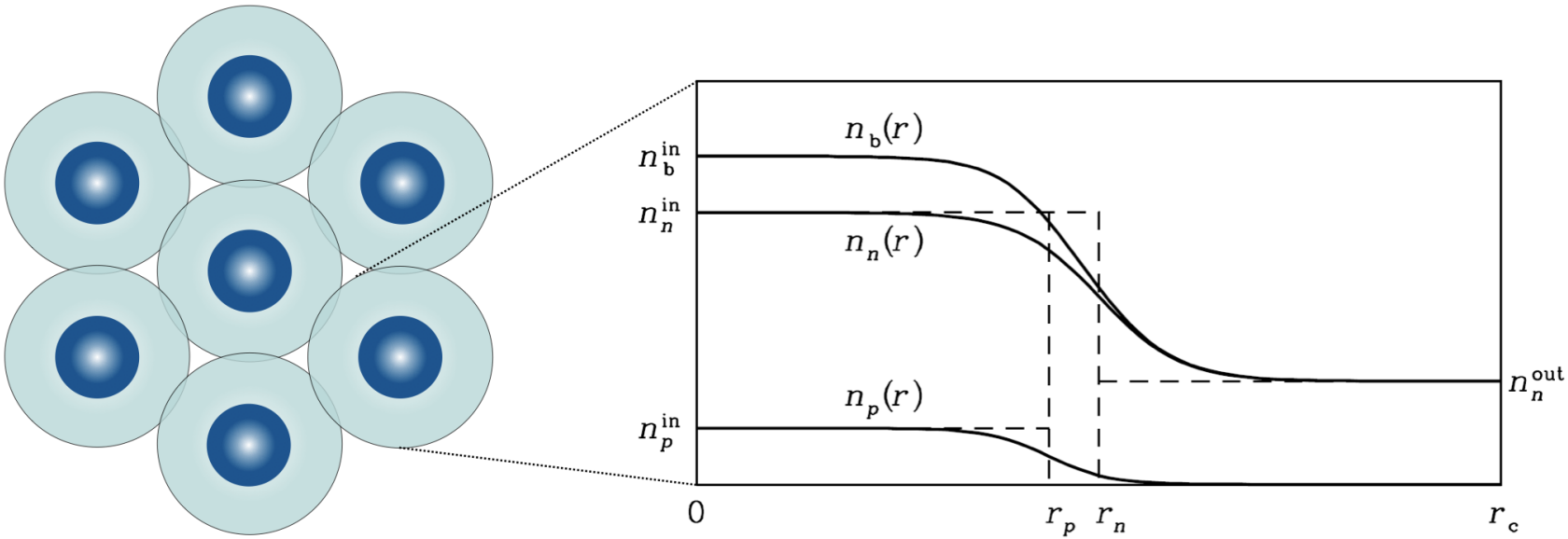

By translational symmetry, it is enough to consider a single **Wigner-Seitz cell** approximated by a sphere.

Such models are computationally very fast and still widely employed.

In principle, bulk and surface energies can be calculated from more microscopic models, but empirical parametrizations are often used.

Nuclei in dense stellar environments

Baym, Bethe and Pethick showed that the existence of nuclei arises from a **detailed balance between surface and Coulomb effects:**

$$E_{\rm surf} = 2E_{\rm Coul}$$

With increasing depth,

- the surface energy decreases due to free neutrons,
- whereas the Coulomb energy increases due to compression.

They anticipated that nuclei would become unstable at some point:

> The fraction of space, u, occupied by nuclei is seen in table 2 to increase monotonically until the nuclei begin to touch. For a bcc lattice the value $u = \sqrt{3}\pi/8 = 0.68$ corresponds to the nuclei just touching. The picture of nuclei as spherical drops is certainly not valid beyond this point. The nuclear parameters A, Z and $n_{\rm N}$, given for $\rho = 2.26 \times 10^{14}$ and 2.39×10^{14} g/cm^3 should be regarded as highly tentative since they are particularly sensitive to the precise way in which the surface energy tends to zero as $n_{\rm n}/n \to 1$. Furthermore, our model has neglected deformations of the nuclei, which become important here. In fact, it might be more favorable, beyond $u = 0.5$, for the nuclei to "turn inside out", that is, for the neutron gas to exist as a lattice of droplets in a sea of nuclear matter.

Baym, Bethe, Pethick, Nucl. Phys. A175, 225 (1971)

Nuclei in neutron-star crust vs ordinary nuclei

Solving the **HF equations in spherical Wigner-Seitz cells** in 1973, Negele&Vautherin found that both types of nuclei look similar:

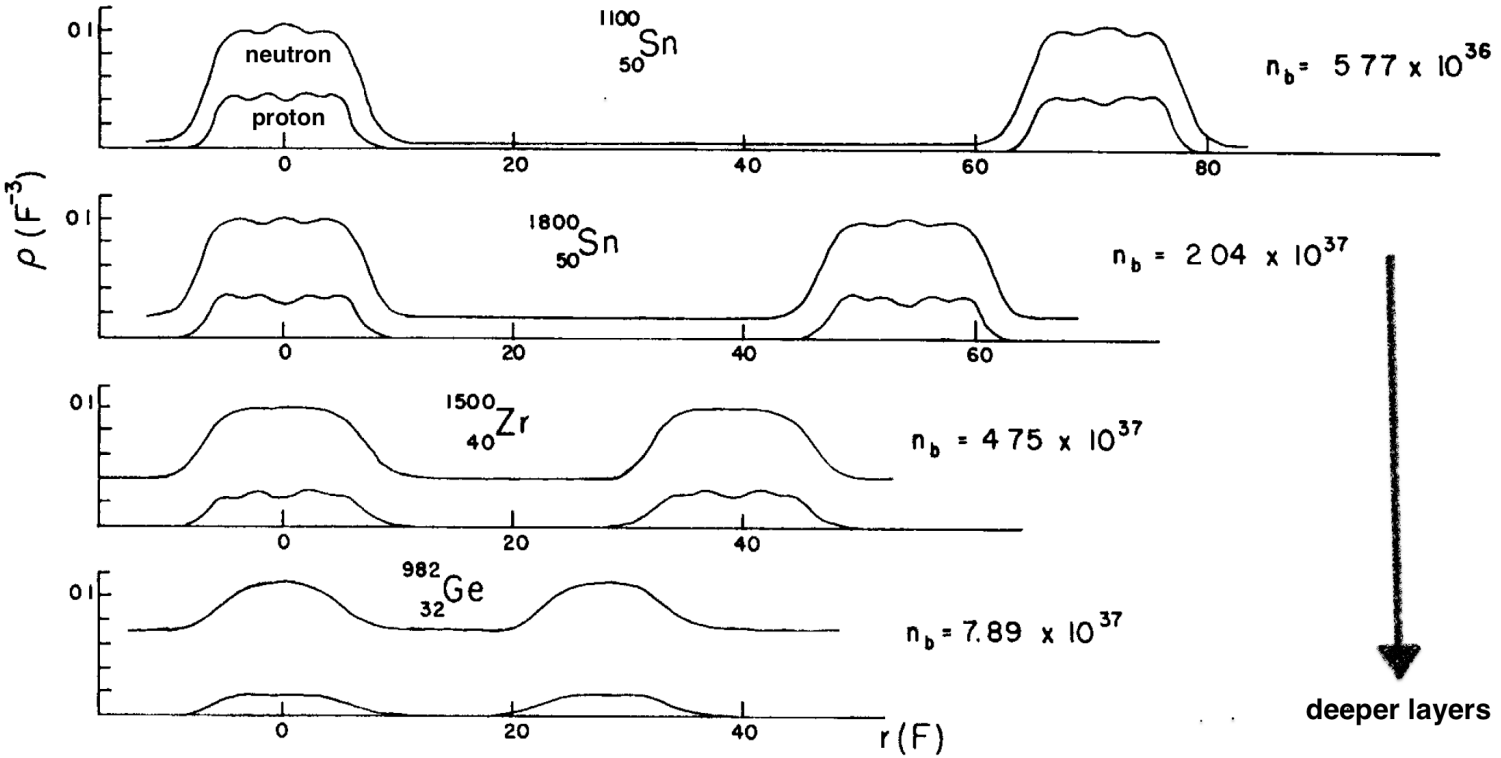

Negele&Vautherin,Nucl.Phys.A207,298(1973)

But they were not able to probe the existence of nuclear bubbles because of numerical instabilities.

Band theory of solids

- The exact Wigner-Seitz cell is not a sphere but a truncated octahedron for a bcc lattice.
- The boundary conditions are dictated by the crystal symmetry.

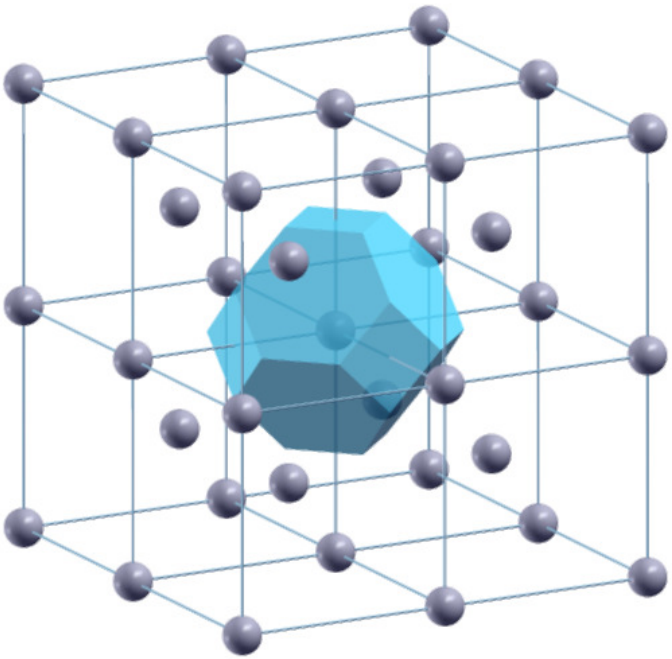

Floquet-Bloch theorem:

$$\varphi_{\alpha \boldsymbol{k}}(\boldsymbol{r}+\boldsymbol{\ell}) = e^{\mathrm{i}\,\boldsymbol{k}\cdot\boldsymbol{\ell}}\varphi_{\alpha \boldsymbol{k}}(\boldsymbol{r})$$

for any lattice translation vector $\boldsymbol{\ell}$.

Quantum numbers:

- α (discrete): rotational symmetry
- $\boldsymbol{k}$: translational symmetry.

Really a **full 3D problem!**

The free neutron energy levels consist of bands analogously to free electrons in metals.

Neutron band structure

Unbound neutron energy levels of zirconium isotopes with $N = 160$ (70 unbound) in a body-centered cubic lattice at $\bar{n} = 4 \times 10^{-4}$ fm^{-3}:

W-S approximation

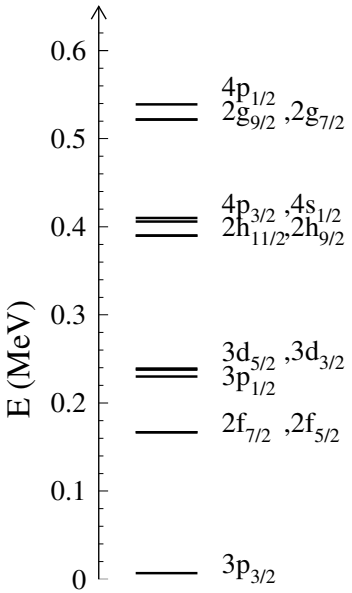

band theory of solids

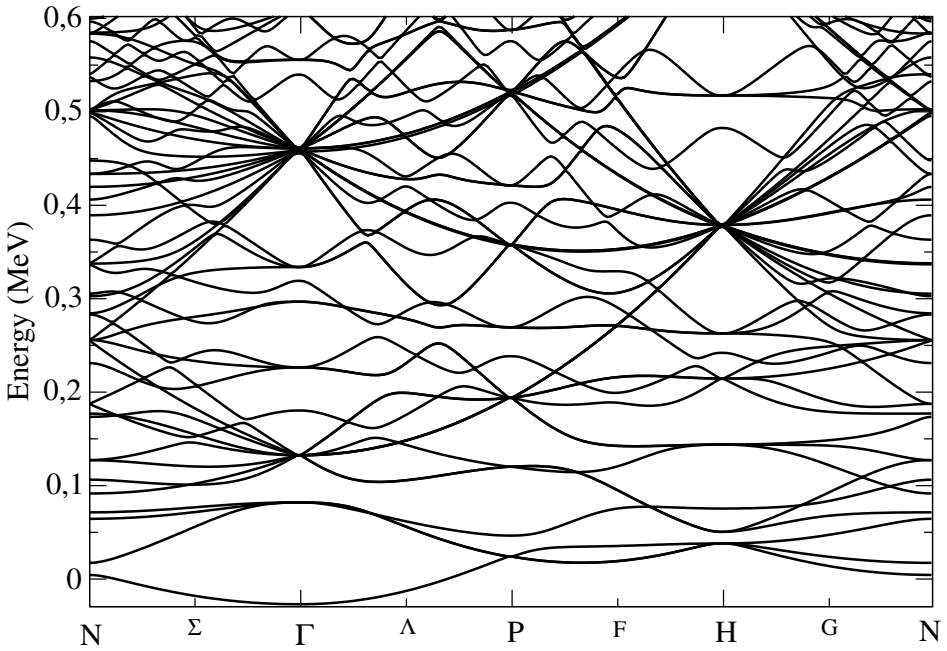

Chamel et al, Phys.Rev.C75, 055806 (2007)

The W-S approach is unreliable beyond ~ 0.02 fm^{-3} due to spurious shell effects induced by approximate boundary conditions.

Chamel et al, PRC75, 055806 (2007); Pastore et al, J.Phys.G44,094003 (2017)

"*Percolating network of linked nuclei*"

In 1982, Ogasawara and Sato speculated that **nuclei may globally connnect** by analogy with percolation networks:

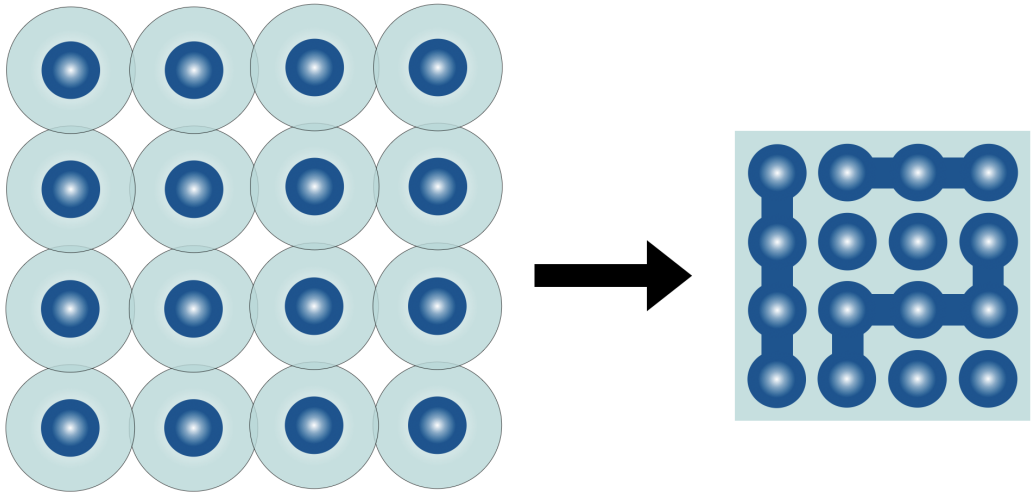

As pictured in Fig. 4, the ratio of the radius of a nucleus to the radius of the Wigner-Seitz cell increases as the density (and/or Y_L) increases. As a result nuclei begin to coalesce in the high density region. This occurs when the ratio R_N/R_C becomes $(8\pi/3)^{1/3}\sqrt{3}/4$ ($=0.88$) or $(4\pi)^{1/3}\sqrt{2}/4$ ($=0.82$) if the nuclei form the b.c.c. lattice, which is the most stable structure of the Coulomb crystal, or the f.c.c. lattice, respectively. If we neglect the Coulomb interaction among nuclei, the percolating network of linked nuclei may be formed when $R_N/R_C \approx (0.3)^{1/3}$ ($=0.67$) from the theories of percolations when the nuclei form no ordered structure and are randomly distributed.[26] Although the effect of the Coulomb repulsion among nuclei[27] could cause to change the critical value of percolation, it is plausible to

Ogasawara&Sato, Prog. Theor. Phys. 68, 222 (1982)

Instability of spherical nuclei in the deep crust

In dense matter, the surface energy of a nucleus is reduced

$$E_{\rm surf} = 2E_{\rm Coul} \approx 2E^0_{\rm Coul}\left(1 - \frac{3}{2}\frac{r_N}{r_c}\right)$$

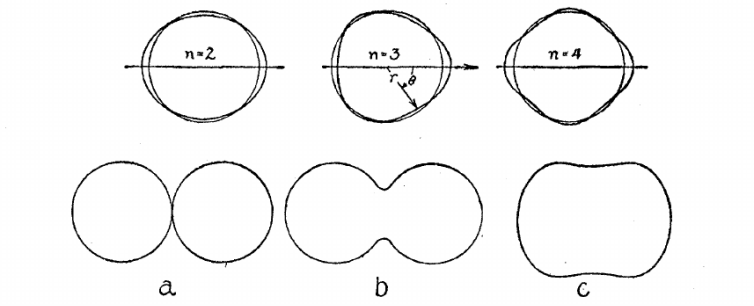

FIG. 2. Small deformations of a liquid drop of the type $\delta r(\theta) = \alpha_n P_n(\cos\theta)$ (upper portion of the figure) lead to characteristic oscillations of the fluid about the spherical form of stable equilibrium, even when the fluid has a uniform electrical charge. If the charge reaches the critical value (10×surface tension×volume)$^{\frac{1}{2}}$, however, the spherical form becomes unstable with respect to even infinitesimal deformations of the type $n=2$. For a slightly smaller charge, on the other hand, a finite deformation (c) will be required to lead to a configuration of *unstable equilibrium*, and with smaller and smaller charge densities the critical form gradually goes over (c, b, a) into that of two uncharged spheres an infinitesimal distance from each other (a).

Applying the **Bohr-Wheeler instability criterion** $E^0_{\rm Coul} \geq 2E_{\rm surf}$

Bohr&Wheeler, Phys.Rev.56,426(1939)

Brandt, Master's thesis (1985)

Pethick&Ravenhall showed that **spherical nuclei in the crust become unstable** when

$$u = (r_N/r_c)^3 \geq 1/8 = 0.125$$

Pethick&Ravenhall, ARNPS45,429(1995)

However, the instability is suppressed by the neglected electrons

Zemlyakov&Chugunov,Particles 5(3), 225(2022)

Nuclear “pasta”: first predictions

Nuclear “pasta” were first studied based on liquid-drop models.

Ravenhall et al., PRL50, 2066 (1983);Hashimoto et al., PTP71, 320 (1984)

Oyamatsu et al., PTP 72, 373 (1984)

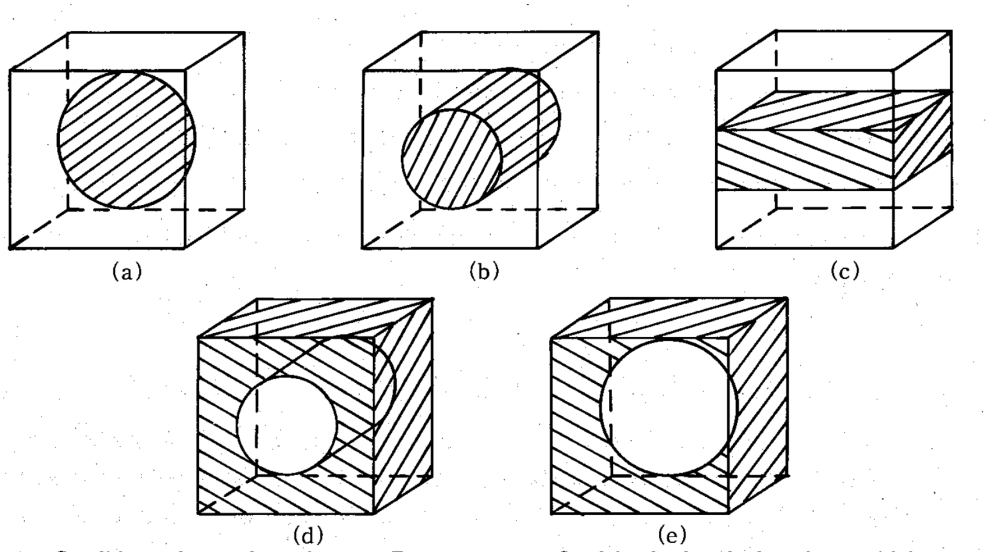

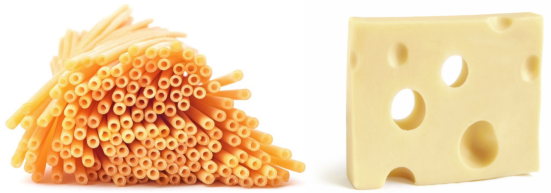

Nuclear “pasta”: first predictions

Nuclear “pasta” were first studied based on liquid-drop models.

Ravenhall et al., PRL50, 2066 (1983);Hashimoto et al., PTP71, 320 (1984)

Oyamatsu et al., PTP 72, 373 (1984)

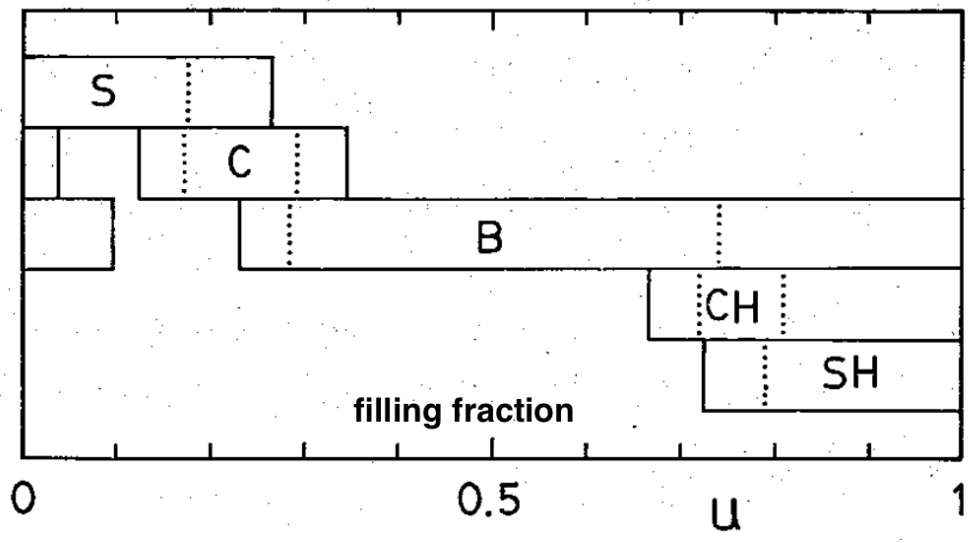

With increasing filling fraction ($u \gtrsim 0.2$): gnocchi (S), spaghetti (C), lasagna (B), bucatini (CH), and Swiss cheese/emmental (SH).

However, the existence of nuclear pasta can be altered by various corrections (e.g., neutron skin, curvature, etc).

Nuclear pasta in neutron stars

According to recent liquid-drop calculations, pasta could represent about **50% of the mass of neutron-star crust**.

e.g. *Newton et al. EpJA58, 69 (2022); Dinh Thi et al., A&A 654, A114 (2021)*

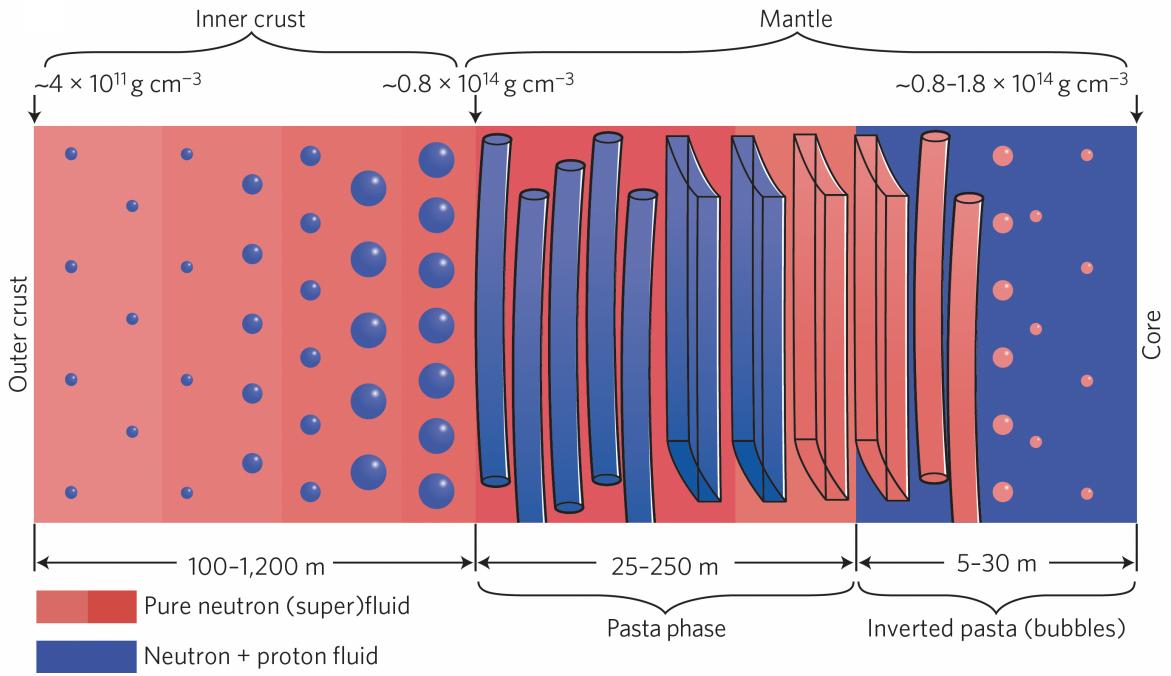

W. G. Newton, Nature Phys. 9, 396 (2013)

pasta could have implications for magnetothermal and dynamical evolutions of neutron stars, as well as gravitational-wave emission.

Formation of nuclear pasta

The formation of nuclear pasta has been explored using large scale molecular dynamics in a box with periodic boundary conditions:

- **classical molecular dynamics** ($N \sim 10^3 - 10^5$)
  pointlike particles interacting through a two-body potential
  Berry et al., PRC94,055801(2016); *Dorso et al., PRC86,055805(2012)*
- **"quantum" molecular dynamics** ($N \sim 10^3$)
  Gaussian wave packets moving (classically) in a mean field.
  Phenomenological antisymmetrisation (Pauli potential).
  Maruyama et al., Prog.Theor.Exp.Phys. 2012,01A201(2012)
- **fermionic molecular dynamics** (very costly, scale as N^4 vs N^2)
  Slater determinants. Few attempts so far.
  Vantournhout et al.,Prog.Part.Nucl.Phys.66,271(2011); *Vantournhout&Feldmeier, J.Phys.Conf.Ser.342,012011(2012)*

Results could be influenced by the geometry of the box and the treatment of Coulomb interactions.
Giménez Molinelli&Dorso,NPA933,306 (2015); *Alcain et al., PRC89,055801(2014)*

Models of nuclear pasta

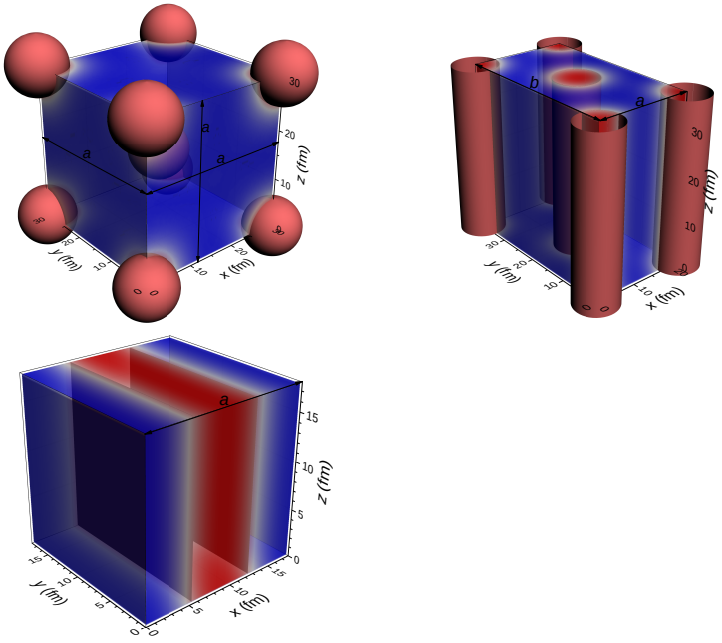

Xia et al,PRC103,055812(2021)

pasta have been mostly studied within

- liquid-drop models,
- (semi)classical models.

Reviews:

Chamel&Haensel, Liv.Rev.Relativ.11, 10 (2008)

Kaplan&Horowitz,Rev.Mod.Phys.89,041002(2017)

Blaschke&Chamel, Astrophys. Space Sci. Lib. 457, eds L. Rezzolla, P. Pizzochero, D. I. Jones, N. Rea, I. Vidaña p. 337-400 (Springer, 2018) arXiv:1803.01836

To which extent do shell effects (magic numbers) and pairing impact the existence of nuclear pasta?

This question can be addressed within the **self-consistent nuclear energy-density functional theory**.

Nuclear energy-density functional theory

Many-body problem reduced to an **effective one-body problem**. This goes beyond the mean-field approximation.

In practice, one must solve the coupled **Hartree-Fock-Bogoliubov (HFB)** equations for both neutrons and protons ($q = n, p$):

$$\sum_{\sigma'} \begin{pmatrix} h'_q(\boldsymbol{r})_{\sigma\sigma'} & \Delta_q(\boldsymbol{r})\delta_{\sigma\sigma'} \\ \Delta_q(\boldsymbol{r})^*\delta_{\sigma\sigma'} & -\sigma\sigma' h'_q(\boldsymbol{r})^*_{-\sigma-\sigma'} \end{pmatrix} \begin{pmatrix} \psi_1^{(q)}(\boldsymbol{r},\sigma') \\ \psi_2^{(q)}(\boldsymbol{r},\sigma') \end{pmatrix} = \mathfrak{E}^{(q)} \begin{pmatrix} \psi_1^{(q)}(\boldsymbol{r},\sigma) \\ \psi_2^{(q)}(\boldsymbol{r},\sigma) \end{pmatrix}$$

$$h'_q(\boldsymbol{r})_{\sigma'\sigma} \equiv \left[-\boldsymbol{\nabla}\cdot\frac{\delta E}{\delta\tau_q(\boldsymbol{r})}\boldsymbol{\nabla} + \frac{\delta E}{\delta n_q(\boldsymbol{r})} - \lambda_q \right]\delta_{\sigma\sigma'} - \mathrm{i}\frac{\delta E}{\delta \boldsymbol{J_q}(\boldsymbol{r})}\cdot\boldsymbol{\nabla}\times\hat{\boldsymbol{\sigma}}_{\sigma'\sigma} + \ldots$$

$n_q(\boldsymbol{r})$, $\tau_q(\boldsymbol{r})$, $\boldsymbol{J_q}(\boldsymbol{r})$, $\Delta_q(\boldsymbol{r})\ldots$ are defined from the density matrices

$$n_q(\boldsymbol{r},\sigma;\boldsymbol{r'},\sigma') = \langle\Psi|c_q(\boldsymbol{r'},\sigma')^\dagger c_q(\boldsymbol{r},\sigma)|\Psi\rangle$$

$$\widetilde{n}_q(\boldsymbol{r},\sigma;\boldsymbol{r'},\sigma') = -\sigma'\langle\Psi|c_q(\boldsymbol{r'},-\sigma')c_q(\boldsymbol{r},\sigma)|\Psi\rangle,$$

Nuclear energy-density functional theory

Many-body problem reduced to an **effective one-body problem**. This goes beyond the mean-field approximation.

In practice, one must solve the coupled **Hartree-Fock-Bogoliubov (HFB)** equations for both neutrons and protons ($q = n, p$):

$$\sum_{\sigma'} \begin{pmatrix} h'_q(\boldsymbol{r})_{\sigma\sigma'} & \Delta_q(\boldsymbol{r})\delta_{\sigma\sigma'} \\ \Delta_q(\boldsymbol{r})^*\delta_{\sigma\sigma'} & -\sigma\sigma' h'_q(\boldsymbol{r})^*_{-\sigma-\sigma'} \end{pmatrix} \begin{pmatrix} \psi_1^{(q)}(\boldsymbol{r},\sigma') \\ \psi_2^{(q)}(\boldsymbol{r},\sigma') \end{pmatrix} = \mathfrak{E}^{(q)} \begin{pmatrix} \psi_1^{(q)}(\boldsymbol{r},\sigma) \\ \psi_2^{(q)}(\boldsymbol{r},\sigma) \end{pmatrix}$$

$$h'_q(\boldsymbol{r})_{\sigma'\sigma} \equiv \left[-\boldsymbol{\nabla}\cdot\frac{\delta E}{\delta\tau_q(\boldsymbol{r})}\boldsymbol{\nabla} + \frac{\delta E}{\delta n_q(\boldsymbol{r})} - \lambda_q \right]\delta_{\sigma\sigma'} - \mathrm{i}\frac{\delta E}{\delta \boldsymbol{J_q}(\boldsymbol{r})}\cdot\boldsymbol{\nabla}\times\hat{\boldsymbol{\sigma}}_{\sigma'\sigma} + \ldots$$

$n_q(\boldsymbol{r})$, $\tau_q(\boldsymbol{r})$, $\boldsymbol{J_q}(\boldsymbol{r})$, $\Delta_q(\boldsymbol{r})\ldots$ are defined from the density matrices

$$n_q(\boldsymbol{r},\sigma;\boldsymbol{r'},\sigma') = \langle\Psi|c_q(\boldsymbol{r'},\sigma')^\dagger c_q(\boldsymbol{r},\sigma)|\Psi\rangle$$

$$\widetilde{n}_q(\boldsymbol{r},\sigma;\boldsymbol{r'},\sigma') = -\sigma'\langle\Psi|c_q(\boldsymbol{r'},-\sigma')c_q(\boldsymbol{r},\sigma)|\Psi\rangle,$$

which in turn depend on $\psi_1^{(q)}(\boldsymbol{r},\sigma)$ and $\psi_2^{(q)}(\boldsymbol{r},\sigma)$: **self-consistency**.

N. Schunck (ed.), EDF Methods for Atomic Nuclei (IOP Publishing, Bristol, 2019)

Description of the inner crust of a neutron star

3D HFB calculations are **computationally very costly**. HF(+BCS) calculations for a few selected densities and proton fractions:

Schuetrumpf & Nazarewicz, PRC92, 045806 (2015); Schuetrumpf et al., PRC100, 045806 (2019); Newton et al., PRC105, 025806 (2022)

Intead, we use the **Extended Thomas-Fermi (ETF)+Strutinsky Integral (SI)** method:

- **semiclassical expansion up to** $\hbar^4$: the energy E becomes a functional of $n_q(\boldsymbol{r})$ and their derivatives only.
- **shell effects and pairing** are added consistently.
- different shapes are allowed: spheres, cylinders, slabs.
- to speed-up the computations, $n_q(\boldsymbol{r})$ are parametrized.

Pearson&Chamel, PRC101,015802(2020); *PRC105,015803(2022)*

The ETFSI method is a **fairly accurate and computationally very fast** approximation to the full HFB equations

Shelley&Pastore, Universe 6, 206 (2020)

Nuclear energy-density functionals

Many functionals are available, but most of them were fitted to a few (doubly magic) nuclei and are not suitable for neutron stars.

Brussels functionals are based on **extended Skyrme and pairing effective interactions**. All were accurately calibrated to a large set of experimental data:

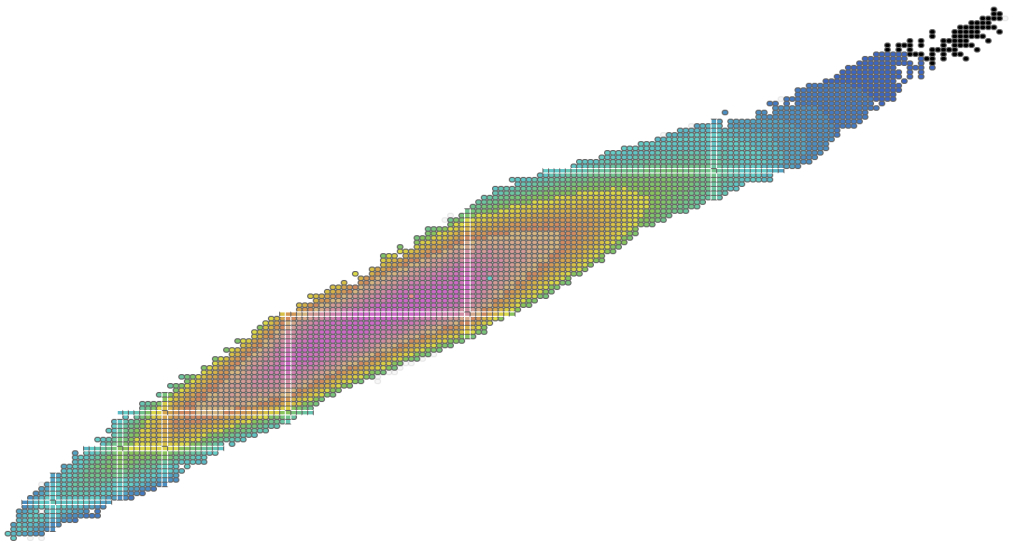

https://www-nds.iaea.org

- $\sim$ 2300 atomic masses from the Atomic Mass Evaluation
- $\sim$ 900 nuclear charge radii

Skyrme effective nucleon-nucleon interactions

Most functionals are constructed from Skyrme **effective contact interactions** in the "mean-field" approximation:

$$
\begin{aligned}
v_{ij} = & \underbrace{t_0(1+x_0P_\sigma)\delta(\boldsymbol{r}_{ij})}_{\text{"long-range" attractive}} + \underbrace{\frac{1}{6}t_3(1+x_3P_\sigma)n(\boldsymbol{r})^\alpha\,\delta(\boldsymbol{r}_{ij})}_{\text{"short-range" repulsive}} \\
& \underbrace{+\frac{1}{2}t_1(1+x_1P_\sigma)\frac{1}{\hbar^2}\left[p_{ij}^2\,\delta(\boldsymbol{r}_{ij})+\delta(\boldsymbol{r}_{ij})\,p_{ij}^2\right]+t_2(1+x_2P_\sigma)\frac{1}{\hbar^2}\boldsymbol{p}_{ij}.\delta(\boldsymbol{r}_{ij})\,\boldsymbol{p}_{ij}}_{\text{"intermediate-range"}} \\
& \underbrace{+\frac{\mathrm{i}}{\hbar^2}W_0(\boldsymbol{\sigma_i}+\boldsymbol{\sigma_j})\cdot\boldsymbol{p}_{ij}\times\delta(\boldsymbol{r}_{ij})\,\boldsymbol{p}_{ij}}_{\text{spin-orbit}} + \underbrace{\frac{1}{2}(1+P_\sigma)v^\pi(\boldsymbol{r})\delta(\boldsymbol{r}_{ij})}_{\text{pairing}}
\end{aligned}
$$

$\boldsymbol{r}_{ij}=\boldsymbol{r}_i-\boldsymbol{r}_j$, $\boldsymbol{r}=(\boldsymbol{r}_i+\boldsymbol{r}_j)/2$, $\boldsymbol{p}_{ij}=-\mathrm{i}\hbar(\nabla_i-\nabla_j)/2$ is the relative momentum, and P_σ is the two-body spin-exchange operator.

The 10 parameters $t_0, x_0 \ldots, W_0$ (plus pairing part) must be fitted to some nuclear data.

Climbing the Jacob's ladder

- **removal of spurious spin-isospin instabilities** (BSk18)

$$v_{ij} \rightarrow v_{ij} + \frac{1}{2}\, t_4(1 + x_4 P_\sigma)\frac{1}{\hbar^2}\left\{p_{ij}^2\, n(\boldsymbol{r})^\beta\, \delta(\boldsymbol{r}_{ij}) + \delta(\boldsymbol{r}_{ij})\, n(\boldsymbol{r})^\beta\, p_{ij}^2\right\}$$
$$+ t_5(1 + x_5 P_\sigma)\frac{1}{\hbar^2}\boldsymbol{p}_{ij} \cdot n(\boldsymbol{r})^\gamma\, \delta(\boldsymbol{r}_{ij})\, \boldsymbol{p}_{ij}$$

Chamel, Goriely, Pearson, PRC80,065804(2009); *PRC82, 045804 (2010)*

- **fit to realistic neutron-matter equations of state** (BSk19-21)

Goriely, Chamel, Pearson, Phys.Rev.C 82, 035804 (2010)

- **fit to different symmetry energies** (BSk22-26)

Goriely, Chamel, Pearson, Phys.Rev.C 88, 024308 (2013)

- **generalized spin-orbit coupling** (BSk29)

$$\mathcal{E}_{\rm so} = \frac{1}{2}\left[\boldsymbol{J} \cdot \boldsymbol{\nabla} n + (1 + y_w)\sum_q \boldsymbol{J_q} \cdot \boldsymbol{\nabla} n_q\right]$$

Goriely, Nucl.Phys.A933, 68 (2015)

- **fit to realistic $^1S_0$ pairing gaps** (BSk30-32)

Chamel et al.,Nucl.Phys.A812, 72(2008); *Chamel, Phys.Rev.C82, 014313(2010)*

Goriely, Chamel, Pearson, Phys.Rev.C93, 034337(2016)

- **new family using a full 3D HFB code** (BSkG1-3)

Grams et al., EPJ A59, 270 (2023)

BSk19-21: neutron-matter constraint

BSk19-21 were simultaneously fitted to three realistic neutron-matter equations of state with different degrees of stiffness:

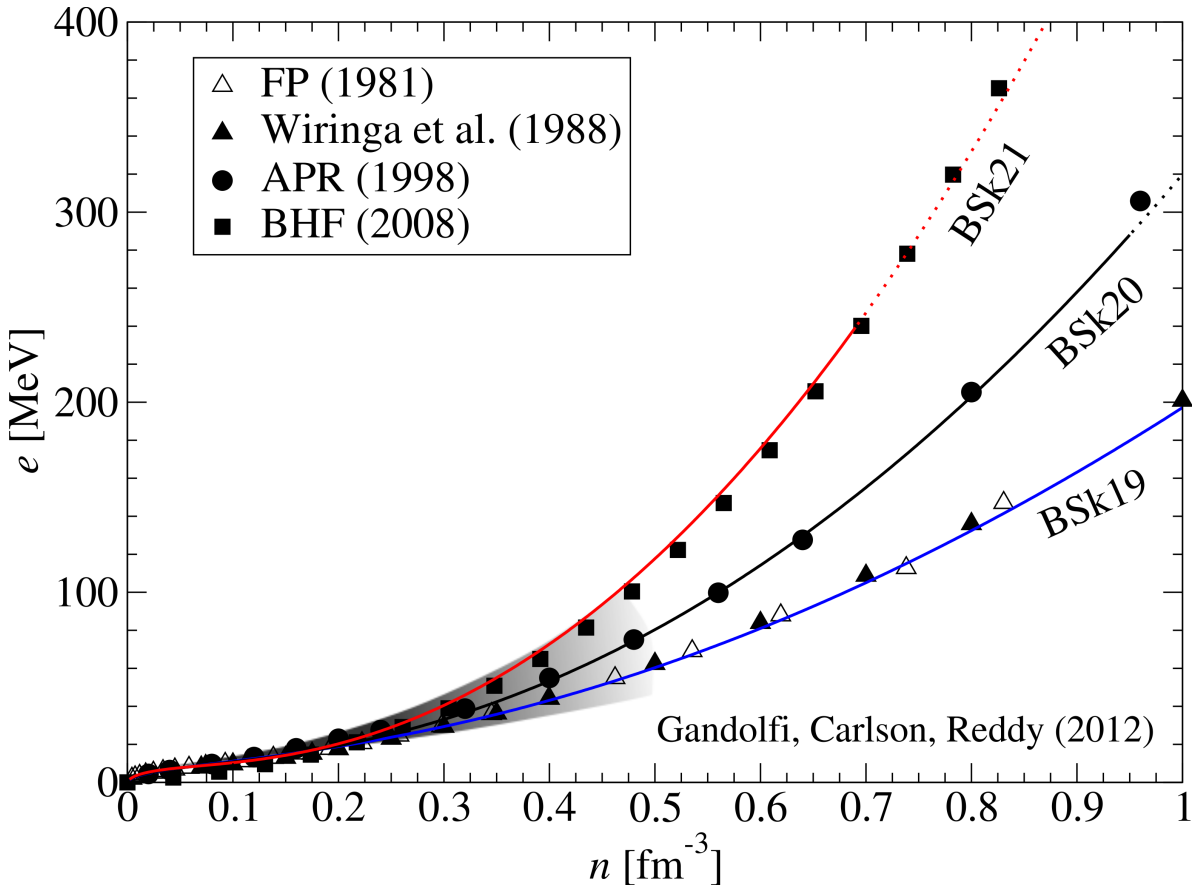

Goriely, Chamel, Pearson, Phys.Rev.C 82, 035804 (2010)

BSk22-26: symmetry-energy constraints

BSk22-26 were further adjusted to different values of $J = S(n_0)$.

	BSk22	BSk23	BSk24	BSk25	BSk26
a_v [MeV]	-16.088	-16.068	-16.048	-16.032	-16.064
n_0 [fm^{-3}]	0.1578	0.1578	0.1578	0.1587	0.1589
J [MeV]	**32.0**	**31.0**	**30.0**	**29.0**	**30.0**
L [MeV]	68.5	57.8	46.4	36.9	37.5
K_{sym}[MeV]	13.0	-11.3	-37.6	-28.5	-135.6
K_v [MeV]	245.9	245.7	245.5	236.0	240.8
K' [MeV]	275.5	275.0	274.5	316.5	282.9
M_s^*/M	0.80	0.80	0.80	0.80	0.80
M_v^*/M	0.71	0.71	0.71	0.74	0.65
NeuM	BHF	BHF	BHF	BHF	APR

Lower and higher values of J were considered but yielded substantially worse fits to atomic masses.

BHF: 'V18' from *Li & Schulze, PRC 78, 028801 (2008)*
APR: 'A18 + δv + UIX*' from *Akmal et al., PRC 58, 1804 (1998)*

BSk22-26: symmetry-energy constraints

The symmetry energy $S(n)$ at lower densities is consistent with various experimental constraints:

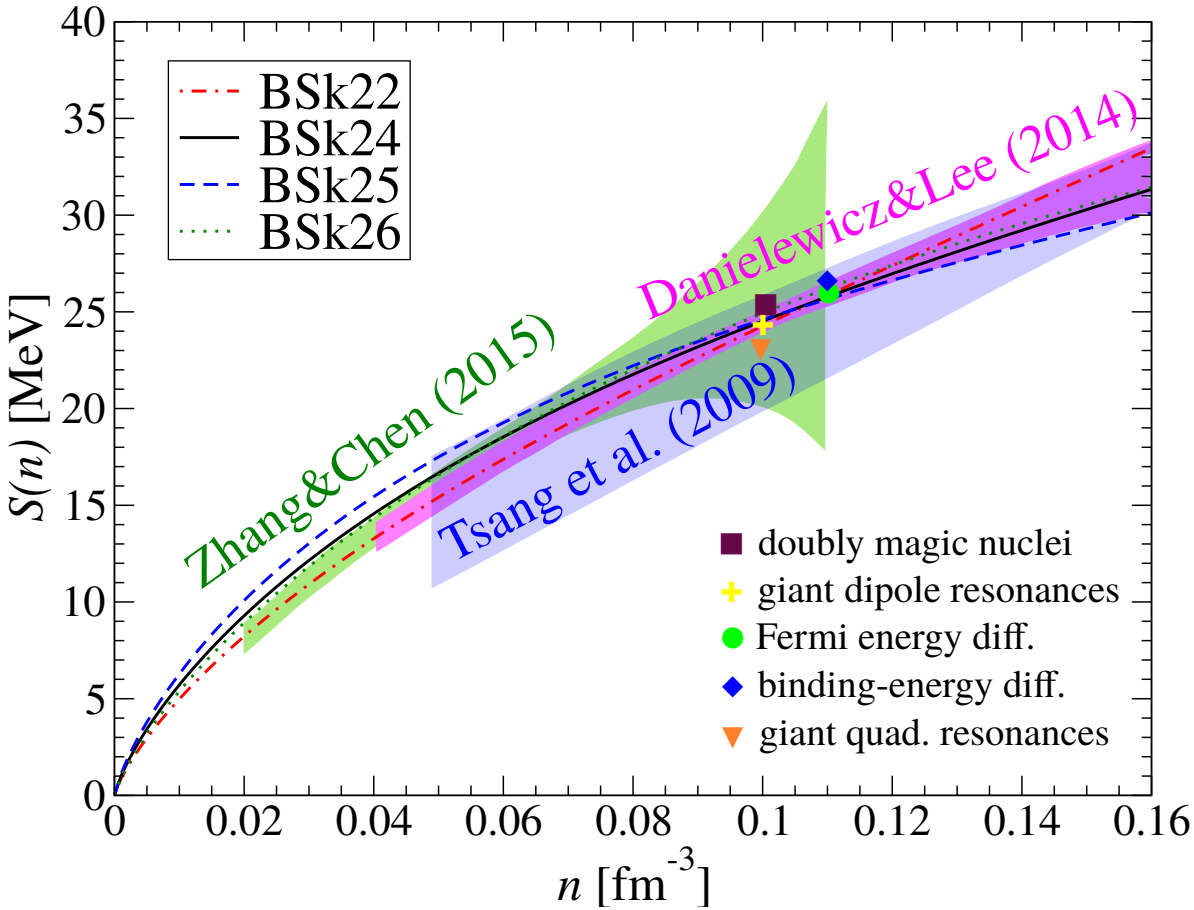

Goriely, Chamel, Pearson, Phys.Rev.C 88, 024308 (2013)

Symmetry energy at higher densities

BSk22-26 mainly differ in their predictions for the symmetry energy at densities encountered in the core of neutron stars:

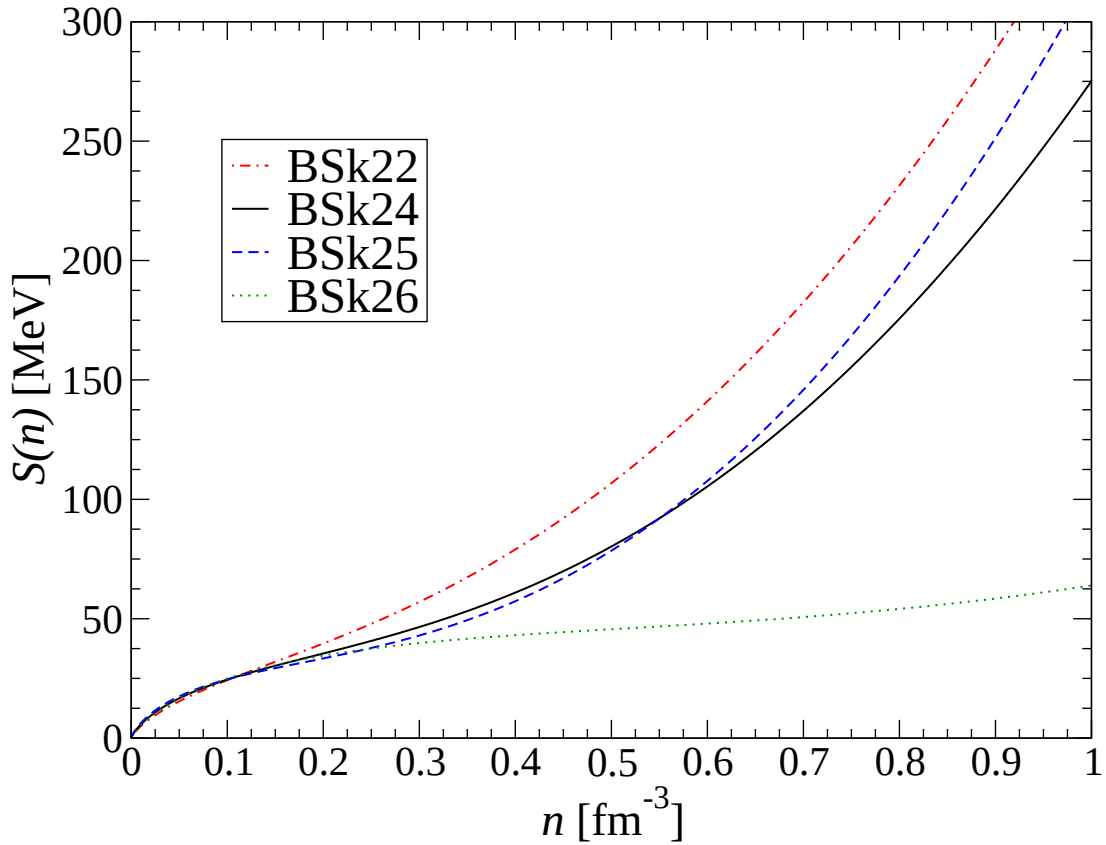

Goriely, Chamel, Pearson, Phys.Rev.C 88, 024308 (2013)

BSk vs chiral EFT

BSk22-26 are in fairly good agreement with recent calculations based on chiral effective-field theory at N3LO from Drischler et al. (2020):

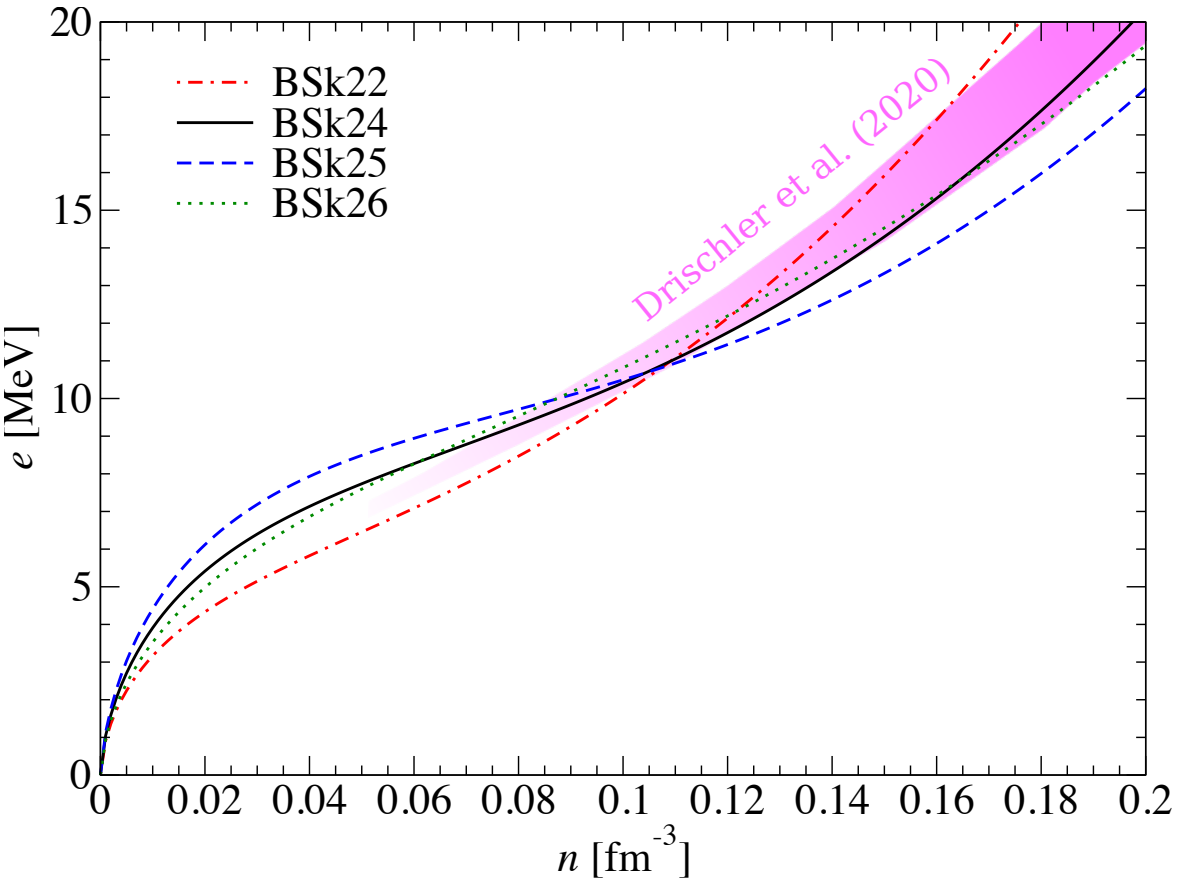

BSk22-26 were NOT fitted to these chiral EFT calculations.

Proton shell effects in stellar environments

The ordinary nuclear shell structure is altered in dense matter: $Z = 28, 82$ disappear, while $40, 58, 92$ appear (quenched spin-orbit).

Energy per nucleon obtained with BSk24 for spherical nuclei:

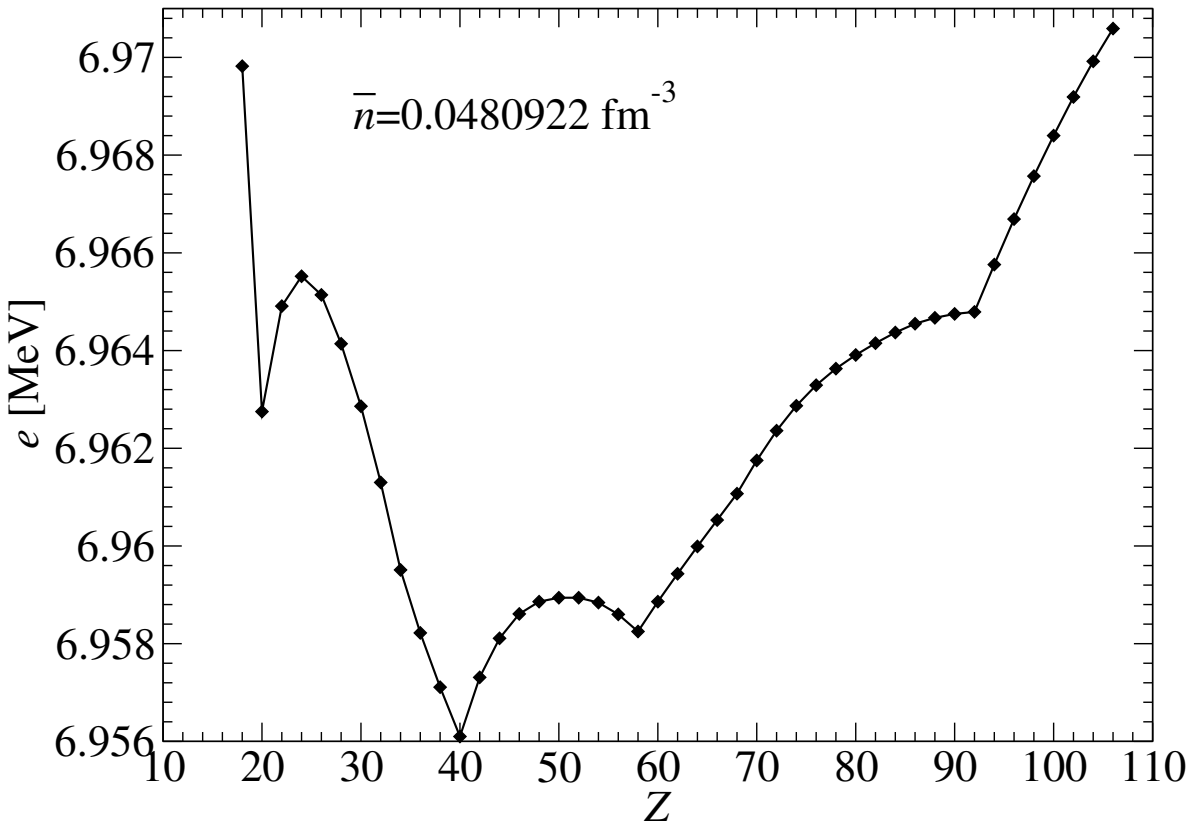

Pearson et al., MNRAS 481, 2994 (2018)

Composition of the inner crust: spherical nuclei

- The composition is strongly influenced by the symmetry energy (the lower $S(\bar{n})$, the lower Z) but also by proton shell effects.
- The crust dissolves at ~ 0.08 fm^{-3}.

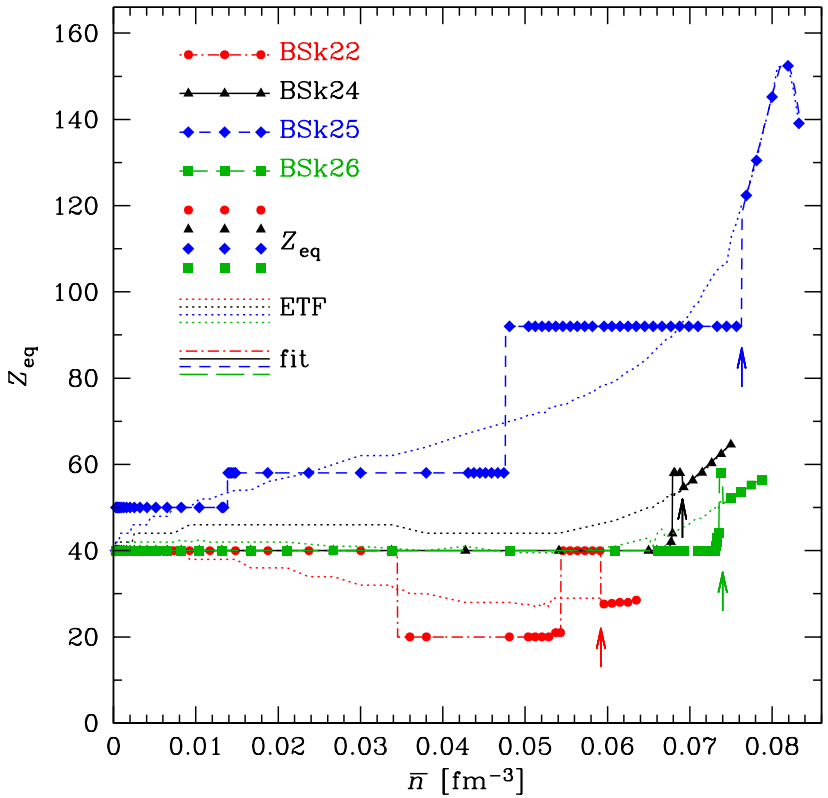

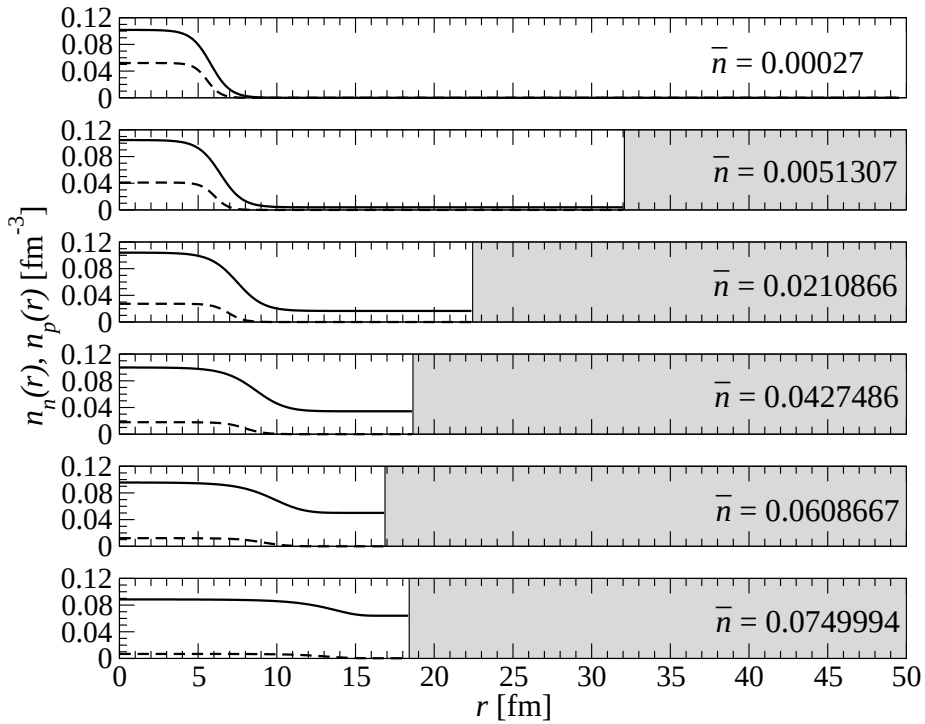

Pearson et al., MNRAS 481, 2994 (2018)

Classical recipe of nuclear pasta (ETF)

Pasta phases are more likely to appear for models with higher values of the symmetry energy at the relevant densities (BSk22 vs BSk25):

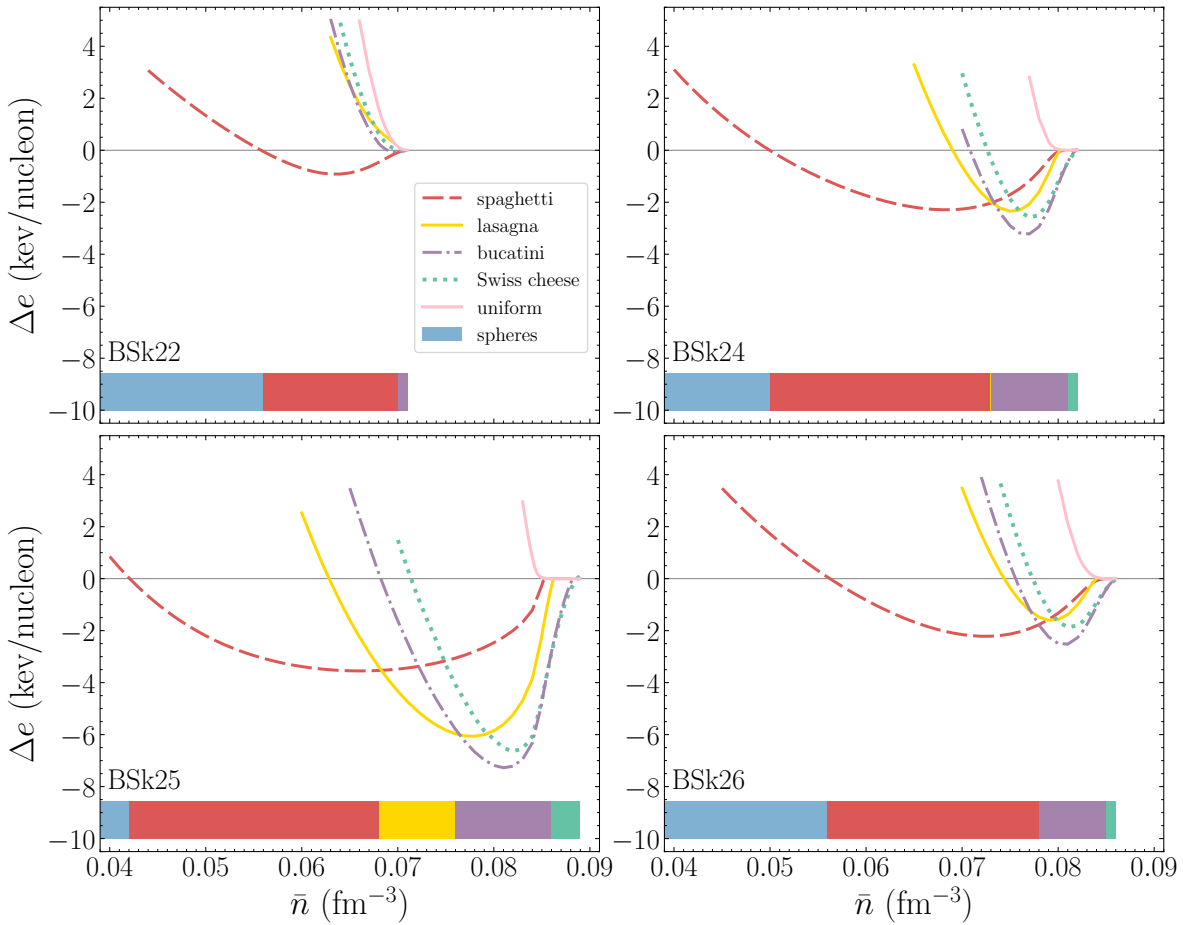

Shchechilin, Chamel, Pearson, Phys. Rev. C108, 025805 (2023)

Quantum recipe of nuclear pasta (ETFSI)

Pasta phases occupy a much narrower range of densities, and correlations with symmetry energy vanish:

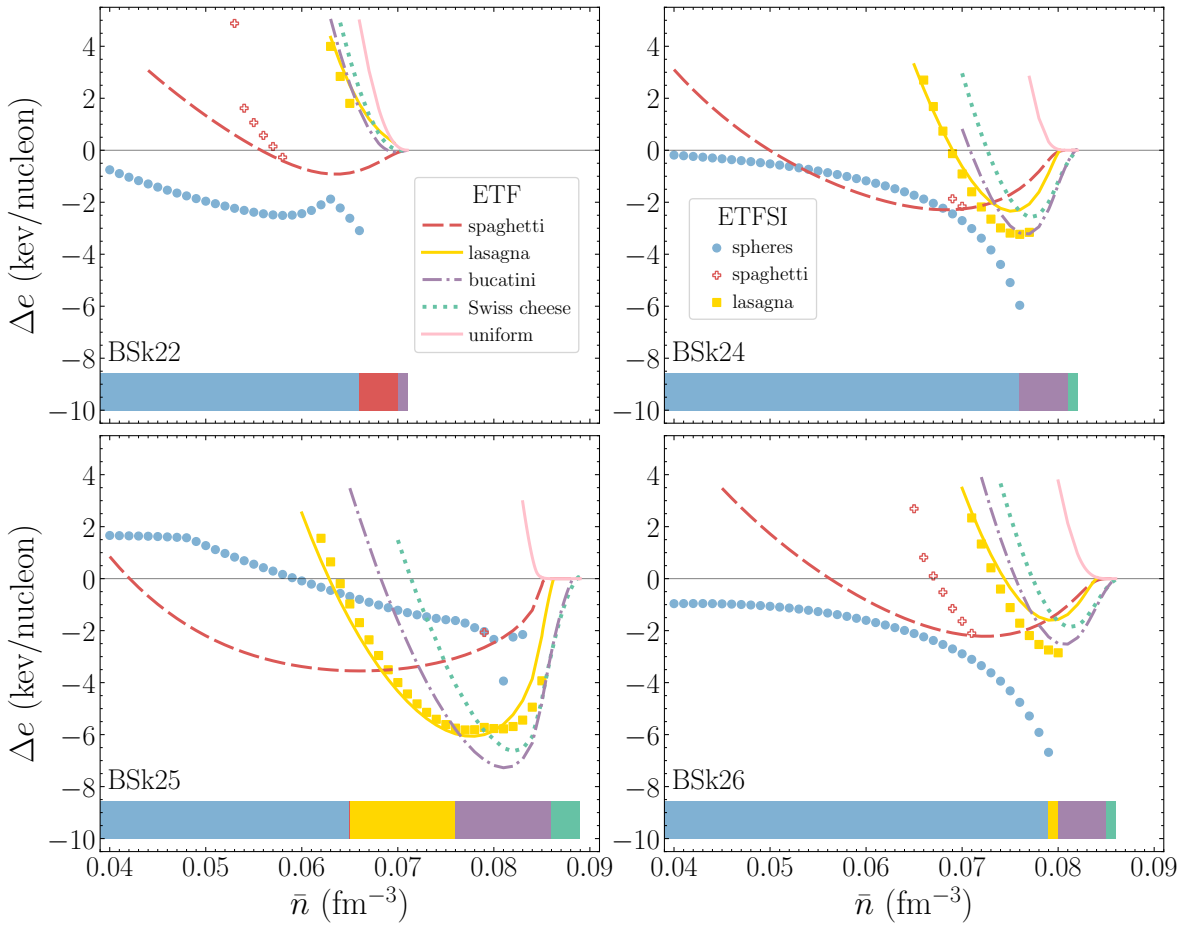

Shchechilin, Chamel, Pearson, Phys. Rev. C108, 025805 (2023)

Nuclear pasta abundances in neutron stars

The pasta mantle shrinks dramatically with shell effects!

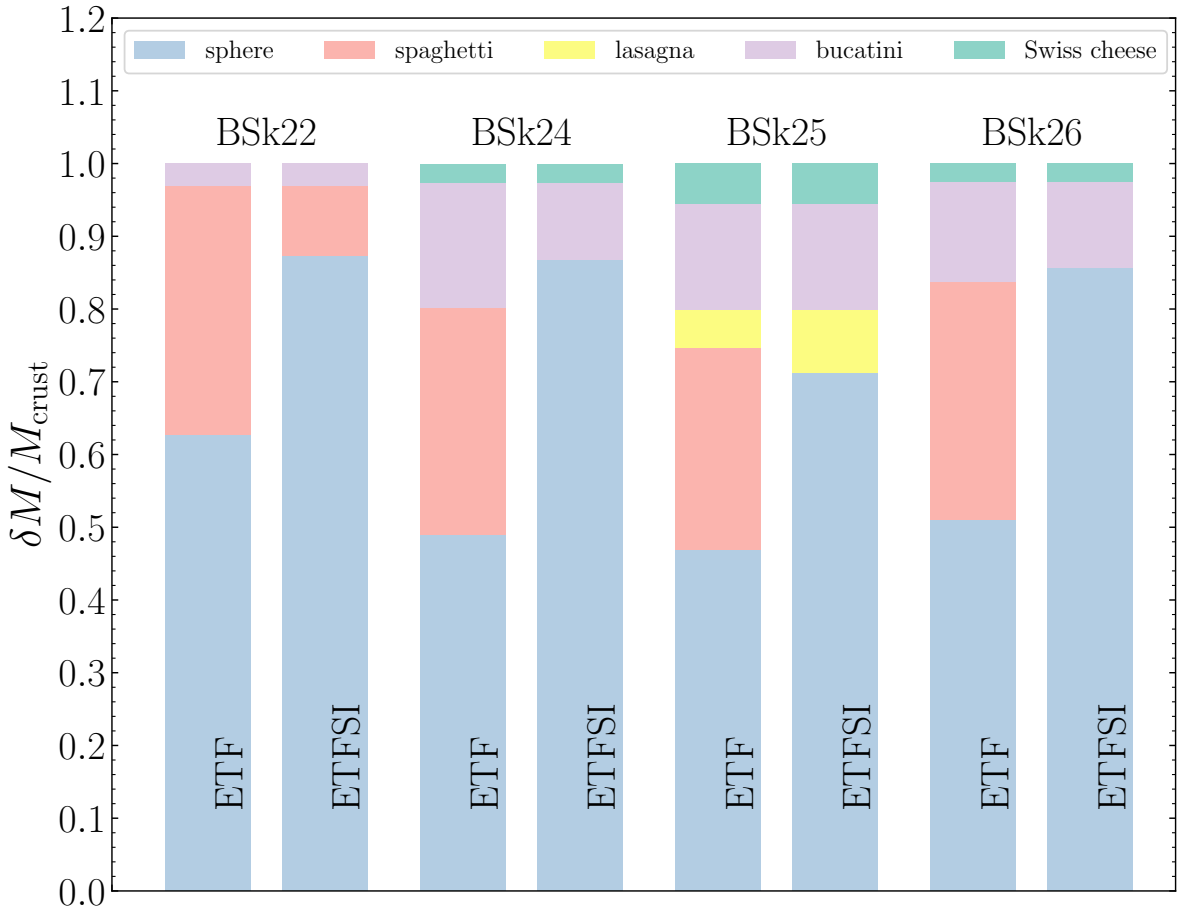

Shchechilin, Chamel, Pearson, Phys. Rev. C108, 025805 (2023)

Role of the nucleon density parametrization

At very high densities, results are sensitive to the choice of the parametrization of $n_q(\xi)$ in the Wigner-Seitz cell of "radius" R.

Writing the nucleon density as $n_q(\xi) = n_{\mathrm{B}q} + n_{\Lambda q} f_q(\xi)$,

the popular ansatz ($n_{\mathrm{B}q}$, $n_{\Lambda q}$, C_q, a_q are free parameters)

$$f_q^{\mathrm{FD}}(\xi) = \frac{1}{1 + \exp\left(\frac{\xi - C_q}{a_q}\right)}$$

does not satisfy the boundary condition $\dfrac{dn_q}{d\xi}(\xi = R) = 0$.

Role of the nucleon density parametrization

At very high densities, results are sensitive to the choice of the parametrization of $n_q(\xi)$ in the Wigner-Seitz cell of "radius" R.

Writing the nucleon density as $n_q(\xi) = n_{\mathrm{B}q} + n_{\Lambda q} f_q(\xi)$,

the ansatz we adopted since 2008

$$f_q^{\mathrm{StrD}}(\xi) = \frac{1}{1 + \exp\left[\left(\frac{C_q - R}{\xi - R}\right)^2 - 1\right] \exp\left(\frac{\xi - C_q}{a_q}\right)}$$

does satisfy $\frac{dn_q}{d\xi}(\xi = R) = 0$ but all derivatives actually vanish.

Onsi et al., Phys.Rev.C77,065805 (2008)

Role of the nucleon density parametrization

At very high densities, results are sensitive to the choice of the parametrization of $n_q(\xi)$ in the Wigner-Seitz cell of "radius" R.

Writing the nucleon density as $n_q(\xi) = n_{\mathrm{B}q} + n_{\Lambda q} f_q(\xi)$,

our new ansatz is

$$f_q^{\mathrm{SoftD}}(\xi) = \frac{1}{1 + \left(\frac{C_q - R}{C_q}\right)^2 \left(\frac{\xi}{\xi - R}\right)^2 \exp\left(\frac{\xi - C_q}{a_q}\right)}$$

satisfies $\dfrac{dn_q}{d\xi}(\xi = 0) = \dfrac{dn_q}{d\xi}(\xi = R) = 0.$

We also consider

$$f_q^{3\mathrm{FD}}(\xi) = f_q^{\mathrm{FD}}(-\xi) + f_q^{\mathrm{FD}}(\xi) + f_q^{\mathrm{FD}}(2R - \xi) - f_q^{\mathrm{FD}}(-R) - 2f_q^{\mathrm{FD}}(R)$$

Role of the nucleon density parametrization

- All parametrizations agree up to the point where pasta first appear at $\bar{n} \approx 0.07$ fm^{-3}.
- The two new parametrizations yield more stable configurations (lower energies).
- Both predict the existence of **gnocchi among pasta**.

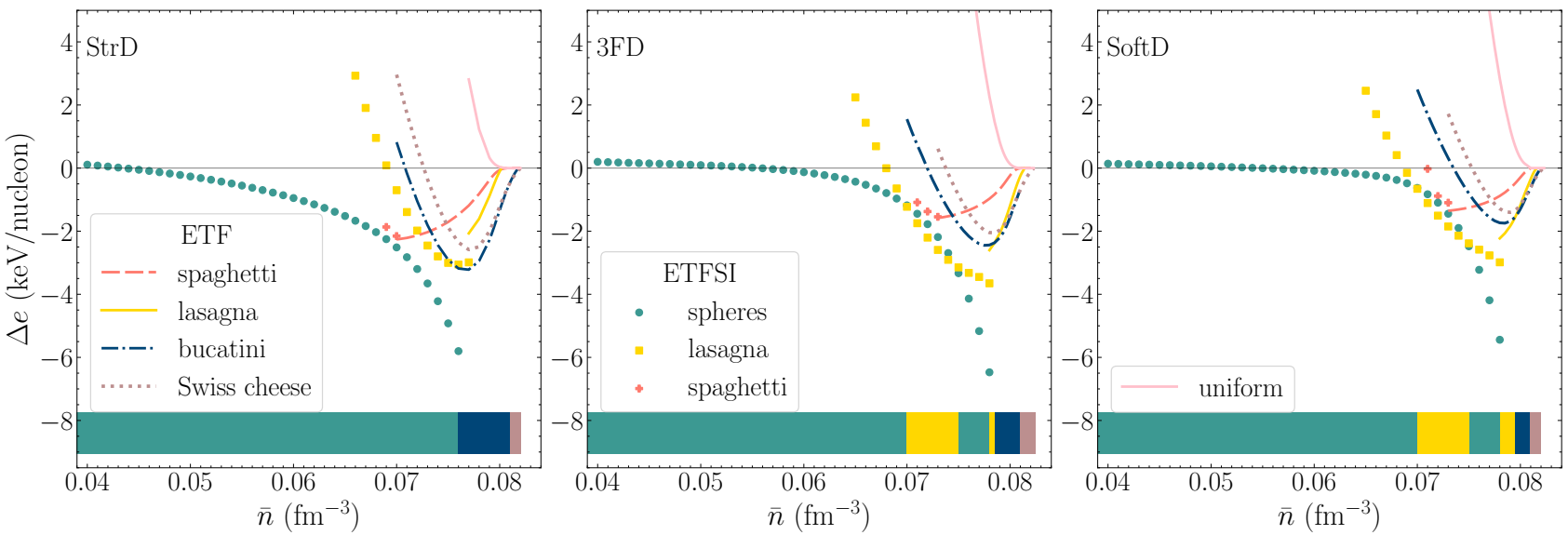

Shchechilin, Chamel, Pearson et al., Phys. Rev. C 109, 055802 (2024)


generated by Microsoft Copilot

Summary and challenges

- Liquid-drop and semiclassical models predict a large amount of pasta in neutron stars (up to 50% of the crust mass).
- Pasta could impact the evolution of neutron stars (e.g. cooling).
- But pasta are suppressed by quantum shell effects.

Full 3D HFB calculations: new pasta shapes? role of pairing?

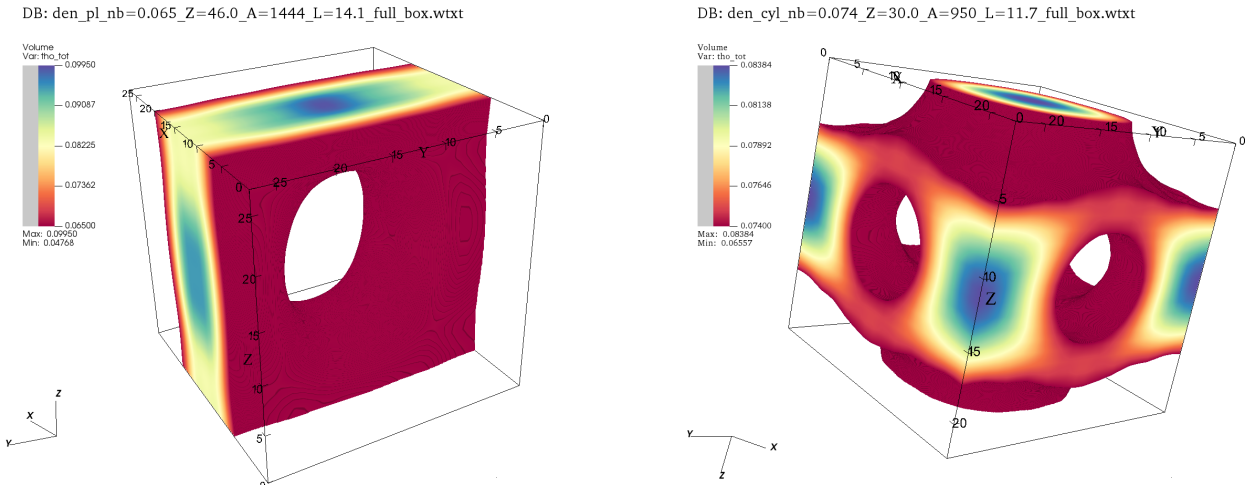

Preliminary results from Nikolai Shchechilin (ULB)

- Cooking of nuclear pasta from the birth of neutron stars: how do they crystallize? glass? can the ground state be reached?
- Role of accretion? Reheating of pasta? Magnetic fields?